
LaserMix for Semi-Supervised LiDAR Semantic Segmentation

Lingdong Kong* Jiawei Ren* Liang Pan Ziwei Liu

S-Lab, Nanyang Technological University

{lingdong001,jiawei011}@e.ntu.edu.sg {liang.pan,ziwei.liu}@ntu.edu.sg

<https://ldkong.com/LaserMix>

Abstract

Densely annotating LiDAR point clouds is costly, which restrains the scalability of fully-supervised learning methods. In this work, we study the underexplored semi-supervised learning (SSL) in LiDAR segmentation. Our core idea is to leverage the strong spatial cues of LiDAR point clouds to better exploit unlabeled data. We propose **LaserMix** to mix laser beams from different LiDAR scans, and then encourage the model to make consistent and confident predictions before and after mixing. Our framework has three appealing properties: **1) Generic**: LaserMix is agnostic to LiDAR representations (*e.g.*, range view and voxel), and hence our SSL framework can be universally applied. **2) Statistically grounded**: We provide a detailed analysis to theoretically explain the applicability of the proposed framework. **3) Effective**: Comprehensive experimental analysis on popular LiDAR segmentation datasets (nuScenes, SemanticKITTI, and ScribbleKITTI) demonstrates our effectiveness and superiority. Notably, we achieve competitive results over fully-supervised counterparts with $2\times$ to $5\times$ fewer labels and improve the supervised-only baseline significantly by 10.8% on average. We hope this concise yet high-performing framework could facilitate future research in semi-supervised LiDAR segmentation. Code will be publicly available².

1 Introduction

LiDAR segmentation is a fundamental task in autonomous driving [1]. It enables autonomous vehicles to semantically perceive the dense 3D structure of the surrounding scenes [2, 3]. However, densely annotating LiDAR point clouds is inevitably expensive and labor-intensive [4, 5], which restrains the scalability of fully-supervised LiDAR segmentation methods. Semi-supervised learning (SSL) that directly leverages the easy-to-acquire unlabeled data is hence a viable and promising solution to achieve scalable LiDAR segmentation [6, 7].

Yet, semi-supervised LiDAR segmentation is still underexplored. Modern SSL frameworks are mainly designed for image recognition [8, 9, 10] and semantic segmentation [11, 12, 13] tasks, which only yield sub-par performance on LiDAR data due to the large modality gap between 2D and 3D. Recent research [14] starts to consider semi-supervised point cloud semantic segmentation as a fresh task, and it designs a novel point contrastive-learning framework. However, their solutions do not differentiate indoor and outdoor scenes and therefore overlook the intrinsic and important properties that only exist in LiDAR point clouds.

In this work, we explore the use of spatial prior for semi-supervised LiDAR segmentation. Unlike the general 2D/3D semantic segmentation tasks, the spatial cues are especially significant in LiDAR

*Equal contribution.

²<https://github.com/ldkong1205/LaserMix>.

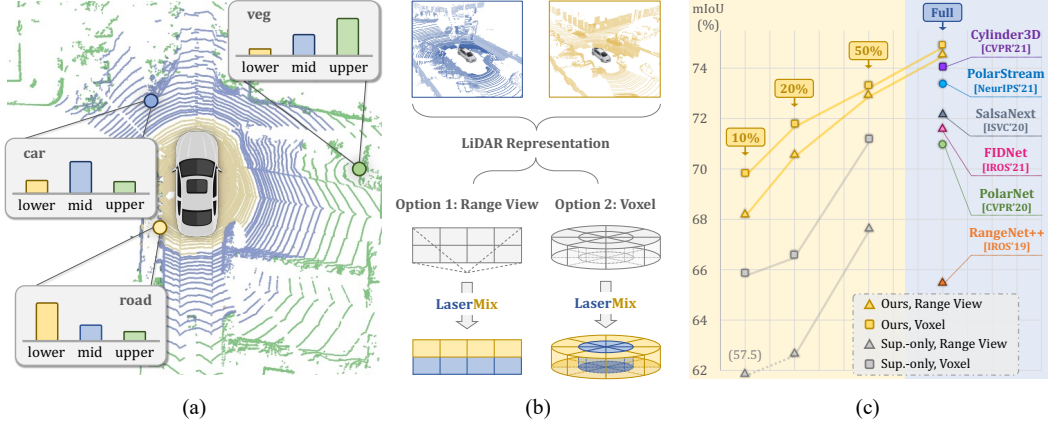


Figure 1: **a)** LiDAR scans contain strong spatial prior. Objects and backgrounds around the ego-vehicle have a patterned distribution on different (lower, middle, upper) laser beams. **b)** Following the scene structure, the proposed LaserMix blends beams from different scans, which is compatible with various popular LiDAR representations. **c)** We achieve superior results over SoTA methods in both low-data (10%, 20%, and 50% labels) and high-data (full labels) regimes on nuScenes [15].

data. In fact, LiDAR point clouds serve as a perfect reflection of the real-world distribution, which is highly dependent on the spatial areas in the LiDAR-centered 3D coordinates. To effectively leverage this strong spatial prior, we propose **LaserMix** to mix laser beams from different LiDAR scans, and then encourage the segmentation model to make consistent and confident predictions before and after mixing. Our SSL framework is statistically grounded, which consists of:

1. Partitioning LiDAR scans into low-variation areas. We observe a strong distribution pattern on laser beams (see Fig. 1(a)) and thus propose the laser partition.
2. Efficiently mixing every area in the scan with foreign data and obtaining model predictions. We propose LaserMix, which mixes the laser-grouped areas from two LiDAR scans in an intertwining way (see Fig. 1(b)), and serves as an efficient LiDAR mixing strategy.
3. Encouraging models to make confident and consistent predictions on the same area in different mixing. We, therefore, propose a mixing-based teacher-student training pipeline.

Despite the simplicity of our overall pipeline, it achieves competitive results over the fully supervised counterpart using $2\times$ to $5\times$ fewer labels (see Fig. 1(c)), and significantly outperforms all prevailing semi-supervised segmentation methods on nuScenes [15] (up to $+5.7\%$ mIoU) and SemanticKITTI [16] (up to $+3.5\%$ mIoU). Moreover, LaserMix directly operates on point clouds so as to be agnostic to different LiDAR representations, *e.g.*, range view [17] and voxel [18]. Therefore, our pipeline can be compatible with existing state-of-the-art (SoTA) LiDAR segmentation methods under various representations [19, 20, 21]. Besides, our pipeline achieves competitive performance using very limited annotations on weak supervision dataset [4]: it achieves 54.4% mIoU on SemanticKITTI [16] using only 0.8% labels, which is on-par with PolarNet [19] (54.3%), RandLA-Net [22] (53.9%), and RangeNet++ [17] (52.2%) using 100% labels. Spatial prior is proven to play a pivotal role in the success of our framework through comprehensive empirical analysis.

To summarize, this work has the following key contributions:

- We present a statistically grounded SSL framework that effectively leverages the spatial cues in LiDAR data to facilitate learning with semi-supervisions.
- We propose LaserMix, a novel and representation-agnostic mixing technique that strives to maximize the “strength” of the spatial cues in our SSL framework.
- Our overall pipeline significantly outperforms previous SoTA methods in both low- and high-data regimes. We hope this work could lay a solid foundation for semi-supervised LiDAR segmentation.

2 Technical Approach

In this section, we first introduce our SSL framework that leverages the spatial prior of LiDAR data by encouraging confidence and consistency in predictions (Sec. 2.1). We then present LaserMix that strives to maximize the “strength” of the spatial prior and mixes LiDAR scans in an efficient manner (Sec. 2.2). Finally, we elaborate the overall pipeline (Sec. 2.3) and present the pseudo-code (Alg. 1).

2.1 Leveraging the Spatial Prior for SSL

Spatial prior formulation. The distribution of real-world objects/backgrounds has a strong correlation to their spatial positions in LiDAR scans. Objects and backgrounds inside a specified spatial area of a LiDAR point cloud follow similar patterns, *e.g.*, the close-range area is most likely *road* while the long-range area consists of *building*, *vegetation*, etc. In another word, there exists a spatial area $a \in A$ where LiDAR points and semantic labels inside the area (denoted as X_{in} and Y_{in} , respectively) will have relatively low variations. Formally, the conditional entropy $H(X_{\text{in}}, Y_{\text{in}}|A)$ is smaller. Therefore, when estimating the parameter θ of the segmentation network \mathcal{G}_θ , we would expect:

$$\mathbb{E}_\theta[H(X_{\text{in}}, Y_{\text{in}}|A)] = c, \quad (1)$$

where c is a small constant. Similar to the classic entropy minimization [23], the constraint in Eq. 1 can be converted to a prior on the model parameter θ using the principle of entropy maximization:

$$P(\theta) \propto \exp(-\lambda H(X_{\text{in}}, Y_{\text{in}}|A)) \propto \exp(-\lambda H(Y_{\text{in}}|X_{\text{in}}, A)), \quad (2)$$

where $\lambda > 0$ is the Lagrange multiplier corresponding to constant c ; $H(X_{\text{in}}|A)$ has been ignored for being independent of the model parameter θ . We consider Eq. 2 as the formal formulation of the spatial prior and discuss how to empirically compute it in the following sections.

Marginalization. To utilize the spatial prior defined in Eq. 2, we empirically compute the entropy $H(Y_{\text{in}}|X_{\text{in}}, A)$ as follows:

$$\hat{H}(Y_{\text{in}}|X_{\text{in}}, A) = \hat{\mathbb{E}}_{X_{\text{in}}, Y_{\text{in}}, A}[P(Y_{\text{in}}|X_{\text{in}}, A) \log P(Y_{\text{in}}|X_{\text{in}}, A)], \quad (3)$$

where $\hat{\cdot}$ denotes the empirical estimation. The end-to-end segmentation model \mathcal{G}_θ usually takes full-sized data as inputs during inference. Therefore, to compute $P(Y_{\text{in}}|X_{\text{in}}, A)$ in Eq. 3, we first pad the data outside the area to obtain the full-sized data. Here we denote the data outside the area as X_{out} ; we then let the model infer $P(Y_{\text{in}}|X_{\text{in}}, X_{\text{out}}, A)$, and finally marginalize X_{out} as follows:

$$P(Y_{\text{in}}|X_{\text{in}}, A) = \hat{\mathbb{E}}_{X_{\text{out}}}[P(Y_{\text{in}}|X_{\text{in}}, X_{\text{out}}, A)]. \quad (4)$$

The generative distribution of the padding $P(X_{\text{out}})$ can be directly obtained from the dataset.

Training. Finally, we train the segmentation model \mathcal{G}_θ using the standard maximum-a-posteriori (MAP) estimation. We maximize the posterior that can be computed by Eq. 2, Eq. 3 and Eq. 4:

$$\begin{aligned} C(\theta) &= L(\theta) - \lambda \hat{H}(Y_{\text{in}}|X_{\text{in}}, A) \\ &= L(\theta) - \hat{\mathbb{E}}_{X_{\text{in}}, Y_{\text{in}}, A}[P(Y_{\text{in}}|X_{\text{in}}, A) \log P(Y_{\text{in}}|X_{\text{in}}, A)], \end{aligned} \quad (5)$$

$$\text{where } P(Y_{\text{in}}|X_{\text{in}}, A) = \hat{\mathbb{E}}_{X_{\text{out}}}[P(Y_{\text{in}}|X_{\text{in}}, X_{\text{out}}, A)].$$

$L(\theta)$ is the likelihood function computed using labeled data, *i.e.*, the conventional supervised learning. Minimizing $\hat{H}(Y_{\text{in}}|X_{\text{in}}, A)$ requires the marginal probability $P(Y_{\text{in}}|X_{\text{in}}, A)$ to be confident, which further requires $P(Y_{\text{in}}|X_{\text{in}}, X_{\text{out}}, A)$ to be both confident and consistent to different X_{out} .

In summary, our proposed SSL framework in Eq. 5 encourages the segmentation model to make confident and consistent predictions at a predefined area, regardless of the data outside the area. The predefined area set A determines the “strength” of the prior. When setting A to the full area (*i.e.*, the whole point cloud), our framework degrades to the classic entropy minimization framework [23].

Implementation. There are three key steps for implementing our framework:

- *Step 1*): Select a partition set A with strong spatial prior;
- *Step 2*): Efficiently compute the marginal probability $P(Y_{\text{in}}|X_{\text{in}}, A)$;
- *Step 3*): Minimize the marginal entropy $\hat{H}(Y_{\text{in}}|X_{\text{in}}, A)$.

We propose a simple yet effective implementation following these steps in the next section.

2.2 LaserMix

Partition. LiDAR sensors have a fixed number (e.g., 32, 64, and 128) of laser beams which are emitted isotropically around the ego-vehicle with predefined inclination angles (see Fig. 2). To obtain a proper set of spatial areas A , we propose to partition the LiDAR point cloud based on laser beams. Specifically, points captured by the same laser beam have a unified inclination angle to the sensor plane. For point i , its inclination ϕ_i is defined as follows:

$$\phi_i = \arctan\left(\frac{p_i^z}{\sqrt{(p_i^x)^2 + (p_i^y)^2}}\right), \quad (6)$$

where (p^x, p^y, p^z) is the Cartesian coordinate of the LiDAR point. Given two LiDAR scans x_1 and x_2 , we first group all points on each scan by their inclination angles. Concretely, to form m non-overlapping areas, a set of $m + 1$ inclination angles $\Phi = \{\phi_0, \phi_1, \phi_2, \dots, \phi_m\}$ will be evenly sampled within the range of the minimum and maximum inlincation angles in the dataset, and the area set $A = \{a_1, a_2, \dots, a_m\}$ can be formed by bounding area a_i in the inclination range $[\phi_{i-1}, \phi_i)$.

Role in our framework: Laser partition effectively “excites” a strong spatial prior in the LiDAR data, as described by *Step 1* in our framework. As shown in Fig. 1(a), we observe an overt pattern in semantic classes detected by each laser beam. Despite being an empirical choice, we will show in later sections that laser partition significantly outperforms other partition choices, including: random points (*MixUp*-like partition [24]), random areas (*CutMix*-like partition [25]), and other heuristics like azimuth α (sensor horizontal direction) or radius r (sensor range directon) partitions.

Mixing. To this end, we propose LaserMix, a simple yet effective LiDAR mixing strategy that can better control the “strength” of the spatial prior. LaserMix mixes the aforementioned laser partitioned areas A from two scans in an intertwining way, *i.e.*, one takes from odd-indexed areas $A_1 = \{a_1, a_3, \dots\}$ and the other takes from even-indexed areas $A_2 = \{a_2, a_4, \dots\}$, so that each area’s neighbor will be from the other scan:

$$\begin{aligned} \tilde{x}_1, \tilde{x}_2 &= \text{LaserMix}(x_1, x_2), \\ \tilde{x}_1 &= \{x_1^{a_1}, x_2^{a_2}, x_1^{a_3}, \dots\}, \\ \tilde{x}_2 &= \{x_2^{a_1}, x_1^{a_2}, x_2^{a_3}, \dots\}, \end{aligned} \quad (7)$$

where $x_i^{a_j}$ is the data crop of x_i in the area a_j . The semantic labels are mixed in the same way.

LaserMix is directly applied to the point clouds and is thus agnostic to the various LiDAR representations [22, 17, 19, 18]. We show LaserMix’s instantiations on *range view* and *voxel* representations (see Fig. 1(b)) since they are currently the most efficient and the best-performing options, respectively.

Role in our framework: LaserMix helps to efficiently compute the marginal probability $P(Y_{\text{in}}|X_{\text{in}}, A)$, as described by *Step 2* in our framework. The cost for directly computing the marginal probability in Eq. 4 on real-world LiDAR data is prohibitive; we need to iterate through all areas in A and all outside data in X_{out} , which requires $|A| \cdot |X_{\text{out}}|$ predictions in total. To reduce the training overhead, we take advantage of the fact that a prediction in an area will be largely affected by its neighboring areas and let X_{out} fill only the neighbors instead of all the remaining areas. LaserMix mixes two scans by *intertwining* the areas so that the neighbors of each area are filled with foreign data. As a result, we obtain the prediction on all areas A of two scans from only two predictions, which on average reduces the cost from $|A|$ to 1. The scan before and after mixing counts as two data fillings, therefore $|X_{\text{out}}| = 2$. Overall, the training overhead is reduced from $|A| \cdot |X_{\text{out}}|$ to 2: only one prediction on original data and one additional prediction on mixed data are required for each LiDAR scan. During training, the memory consumption for a batch will be $2\times$ compared to a standard SSL framework, and the training speed will not be affected.

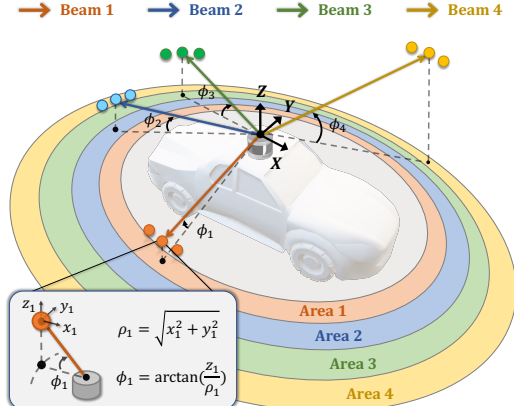


Figure 2: Laser partition example. We group points whose inclinations ϕ are within the same inclination range into the same area a .

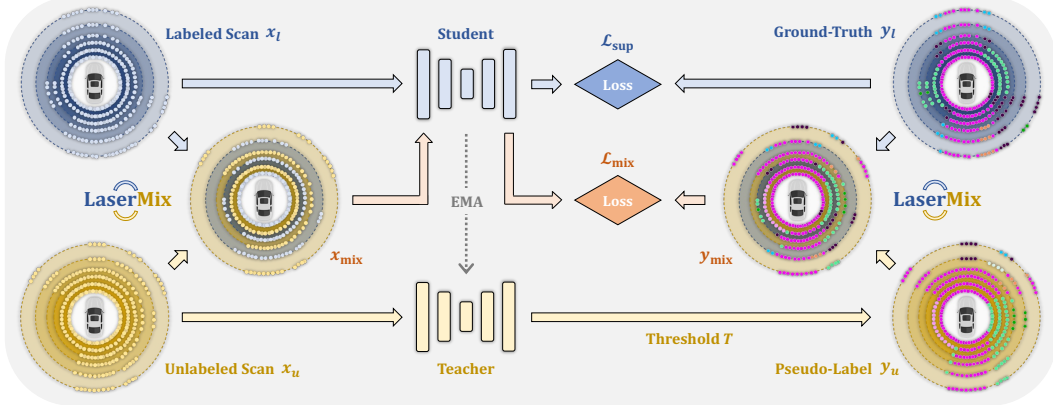


Figure 3: Framework overview. Labeled scan x_l is fed into the Student net to compute the supervised loss \mathcal{L}_{sup} (w/ ground-truth y_l). Unlabeled scan x_u and the generated pseudo-label y_u are mixed with (x_l, y_l) via LaserMix (Sec. 2.2) to produce mixed data $(x_{\text{mix}}, y_{\text{mix}})$, which is then fed into the Student net to compute the mix loss \mathcal{L}_{mix} . Additionally, we adopt the EMA update in [26] for the Teacher net and compute the mean teacher loss \mathcal{L}_{mt} over Student net’s and Teacher net’s predictions.

2.3 Overall Pipeline

We show the overall framework in Fig. 3 and the pseudo-code in Alg. 1. There are two branches in our pipeline, one Student net \mathcal{G}_θ^s and one Teacher net \mathcal{G}_θ^t . During training, a batch is composed of half labeled data and half unlabeled data. We collect the predictions from both \mathcal{G}_θ^s and \mathcal{G}_θ^t , and produce pseudo-labels from Teacher net’s prediction with a predefined confidence threshold T . For labeled data, we compute the cross-entropy loss between the Student net’s prediction and the ground-truth as \mathcal{L}_{sup} . For unlabeled data, LaserMix blends every scan with a random labeled scan, together with their pseudo-label or ground-truth. Then, we let \mathcal{G}_θ^s predict on the mixed data and compute the cross-entropy loss \mathcal{L}_{mix} (w/ mixed labels). The point-wise cross-entropy loss for a scan x and its corresponding ground-truth/pseudo-label y on the segmentation net \mathcal{G}_θ is defined as:

$$\mathcal{L}_{\text{ce}} = \frac{1}{|x|} \sum_{i=1}^{|x|} \text{CrossEntropy}(y^{(i)}, \mathcal{G}_\theta^{(i)}(x)), \quad (8)$$

where (i) denotes the i -th point. Moreover, we adopt the mean teacher idea in [26] and use Exponential Moving Average (EMA) to update the weights of \mathcal{G}_θ^t from \mathcal{G}_θ^s , and compute the L2 loss between their predictions as \mathcal{L}_{mt} :

$$\mathcal{L}_{\text{mt}} = \|\mathcal{G}_\theta^s(x) - \mathcal{G}_\theta^t(x)\|_2^2, \quad (9)$$

where $\|\cdot\|$ denotes the L2 norm. The overall loss function will be:

$$\mathcal{L} = \mathcal{L}_{\text{sup}} + \lambda_{\text{mix}} \mathcal{L}_{\text{mix}} + \lambda_{\text{mt}} \mathcal{L}_{\text{mt}}, \quad (10)$$

where λ_{mix} and λ_{mt} are loss weights. We use the Teacher net during inference as it empirically gives more stable results. There will be no extra inference overhead in our framework.

Role in our framework: Our overall pipeline minimizes the marginal entropy, as described by Step 3 in our framework. Since the objective for minimizing the entropy has a hard optimization landscape, pseudo-labeling is a common resort in practice [27]. Unlike conventional pseudo-label optimization in SSL that only aims to encourage the predictions to be confident, minimizing the marginal entropy requires all predictions to be both confident and consistent. Therefore, we use the ground-truth and pseudo-label as an anchor and encourage the model’s predictions to be confident and consistent with these supervision signals.

Algorithm 1 Pseudo-code for one training iteration in our SSL framework.

```
1: Input: Shuffled labeled batch  $(X_l, Y_l) = \{(x_l^{(b)}, y_l^{(b)}); b \in (1, \dots, B)\}$ , shuffled unlabeled batch  $X_u = \{x_u^{(b)}; b \in (1, \dots, B)\}$ , threshold  $T$ , loss weights  $\lambda_{\text{mix}}$  and  $\lambda_{\text{mt}}$ , Student and Teacher nets.
2: for  $b = 1$  to  $B$  do
3:    $x_{\text{mix}}^{(2b-1)}, x_{\text{mix}}^{(2b)} = \text{LaserMix}(x_l^{(b)}, x_u^{(b)})$  // LaserMix data
4: end for
5:  $X_{\text{mix}} = \{x_{\text{mix}}^{(i)}; i \in (1, \dots, 2B)\}$ 
6:  $S_l, S_u, S_{\text{mix}} = \text{Student}(\text{Concat}(X_l, X_u, X_{\text{mix}}))$  // Student net prediction scores
7:  $\hat{S}_l, \hat{S}_u = \text{Teacher}(\text{Concat}(X_l, X_u))$  // Teacher net prediction scores
8:  $Y_u = \text{PseudoLabel}(\hat{S}_u, T)$  // Produce pseudo-label from scores larger than threshold
9: for  $b = 1$  to  $B$  do
10:   $y_{\text{mix}}^{(2b-1)}, y_{\text{mix}}^{(2b)} = \text{LaserMix}(y_l^{(b)}, y_u^{(b)})$  // LaserMix label
11: end for
12:  $Y_{\text{mix}} = \{y_{\text{mix}}^{(i)}; i \in (1, \dots, 2B)\}$ 
13:  $L_{\text{sup}} = \text{CrossEntropy}(S_l, Y_l)$  // Supervised loss
14:  $L_{\text{mix}} = \text{CrossEntropy}(S_{\text{mix}}, Y_{\text{mix}})$  // Mix loss
15:  $L_{\text{mt}} = \text{L2}(\text{Concat}(S_l, S_u), \text{Concat}(\hat{S}_l, \hat{S}_u))$  // Mean Teacher loss
16:  $L = L_{\text{sup}} + \lambda_{\text{mix}} L_{\text{mix}} + \lambda_{\text{mt}} L_{\text{mt}}$ 
17: Backward(L), Update(Student), UpdateEMA(Teacher)
```

3 Experiments

3.1 Experimental Settings

Protocol. We follow the Realistic Evaluation Protocol [28] when building the benchmark. Specifically, all experiments share the same backbones and are within the same codebase. All configurations and data augmentations are unified to ensure a fair comparison among different SSL algorithms.

Data. We build the LiDAR SSL benchmark upon nuScenes [15], SemanticKITTI [16], and ScribbleKITTI [4]. nuScenes [15] and SemanticKITTI [16] are the two most popular LiDAR segmentation datasets, with 29130 and 19130 training scans and 6019 and 4071 validation scans, respectively. ScribbleKITTI [4] is a recent variant of SemanticKITTI [16], which contains the same number of scans but is annotated with scribbles (approximately 8% valid semantic labels) rather than dense annotations. For all three sets, we uniformly sample 1%, 10%, 20%, and 50% labeled training scans and assume the remaining ones as unlabeled.

Implementation details. We use compact versions of FIDNet [21] and Cylinder3D [18] for the *range view* option and the *voxel* option, respectively. The input resolution of the range images is set as 64×2048 for SemanticKITTI [16] and ScribbleKITTI [4], and 32×1920 for nuScenes [15]. The voxel resolution is fixed as $[240, 180, 20]$ for all three sets. The number of spatial areas m in LaserMix is uniformly sampled from 1 to 6. We denote the supervised-only baseline as *sup.-only*. Due to the lack of LiDAR SSL works [14], we also compare SoTA consistency regularization [26, 13, 29] and entropy minimization [30] methods from semi-supervised image segmentation. We report the intersection-over-union (IoU) scores over each semantic class and the mean IoU (mIoU) scores over all classes in our experiments. All experiments are implemented using PyTorch on NVIDIA Tesla V100 GPUs with 32GB RAM. Please refer to our Appendix for more details.

3.2 Comparative Studies

Improvements over baseline. Tab. 1 benchmarks results on nuScenes [15], SemanticKITTI [16], and ScribbleKITTI [4]. For all three sets under different data splits, we observe significant improvements of our approaches over the *sup.-only* baseline. Such gains are especially evident in *range view*, which reach up to 11.2% mIoU. We also observe constant improvements for the *voxel* option, which provide on average 4.1% mIoU gains over all splits across all sets. The results verify the effectiveness of our framework and further highlight the importance of leveraging unlabeled data in LiDAR segmentation.

Comparison with SoTA. We compare GPC [14], the SoTA 3D SSL method tested on SemanticKITTI [16]. The results in Tab. 2 show that our method exhibits much better results than GPC [14],

Repr.	Method	nuScenes [15]				SemanticKITTI [16]				ScribbleKITTI [4]			
		1%	10%	20%	50%	1%	10%	20%	50%	1%	10%	20%	50%
Range View	<i>Sup.-only</i>	38.3	57.5	62.7	67.6	36.2	52.2	55.9	57.2	33.1	47.7	49.9	52.5
	MeanTeacher [26]	42.1	60.4	65.4	69.4	37.5	53.1	56.1	57.4	34.2	49.8	51.6	53.3
	CBST [30]	40.9	60.5	64.3	69.3	39.9	53.4	56.1	56.9	35.7	50.7	52.7	54.6
	CutMix-Seg [29]	43.8	63.9	64.8	69.8	37.4	54.3	56.6	57.6	36.7	50.7	52.9	54.3
	CPS [13]	40.7	60.8	64.9	68.0	36.5	52.3	56.3	57.4	33.7	50.0	52.8	54.6
Voxel	LaserMix (Ours)	49.5	68.2	70.6	73.0	43.4	58.8	59.4	61.4	38.3	54.4	55.6	58.7
	$\Delta \uparrow$	+11.2	+10.7	+7.9	+5.4	+7.2	+6.6	+3.5	+4.2	+5.2	+6.7	+5.7	+6.2
	<i>Sup.-only</i>	50.9	65.9	66.6	71.2	45.4	56.1	57.8	58.7	39.2	48.0	52.1	53.8
Voxel	MeanTeacher [26]	51.6	66.0	67.1	71.7	45.4	57.1	59.2	60.0	41.0	50.1	52.8	53.9
	CBST [30]	53.0	66.5	69.6	71.6	48.8	58.3	59.4	59.7	41.5	50.6	53.3	54.5
	CPS [13]	52.9	66.3	70.0	72.5	46.7	58.7	59.6	60.5	41.4	51.8	53.9	54.8
	LaserMix (Ours)	55.3	69.9	71.8	73.2	50.6	60.0	61.9	62.3	44.2	53.7	55.1	56.8
$\Delta \uparrow$		+4.4	+4.0	+5.2	+2.0	+5.2	+3.9	+4.1	+3.6	+5.0	+5.7	+3.0	+3.0

Table 1: Benchmarking results for methods with the LiDAR *range view* and *voxel* representations. All mIoU scores are given in percentage (%). The best result for each split is highlighted in **bold**.

Method	5%	10%	20%	30%	40%
GPC [14]	41.8	49.9	58.8	59.4	59.9
Ours (RV)	54.6	58.8	59.4	60.1	60.8
$\Delta \uparrow$	+12.8	+8.9	+0.6	+0.7	+0.9
Ours (Voxel)	56.7	60.0	61.9	62.1	62.3
$\Delta \uparrow$	+14.9	+10.1	+3.1	+1.7	+1.4

Table 2: Comparison to state-of-the-art 3D SSL method on the *val* set of SemanticKITTI [16]. All mIoU scores are given in percentage.

#	\mathcal{L}_{mt}	\mathcal{L}_{mix}	SS	TS	1%	10%	20%	50%
(1)	✓				42.1	60.4	65.4	69.4
(2)		✓	✓		45.6	64.3	67.8	71.6
		✓	✓	✓	47.0	65.5	69.5	72.0
(3)		✓		✓	46.0	64.1	69.5	72.3
	✓	✓		✓	49.5	68.2	70.6	73.0

Table 3: Ablation results (mIoU in percentage) on nuScenes [15] *val* set. (1) Baseline [26]; (2) Student supervision (SS); (3) Teacher supervision (TS).

especially in scenarios where very few annotations are available. We also reimplement popular SSL algorithms from the image segmentation domain and show their results in Tab. 1. We find that these methods, albeit competitive in 2D, only yield sub-par performance in the LiDAR SSL benchmark, highlighting the importance of exploiting the LiDAR data structure. The comparison between prevailing methods in Fig. 1(c) shows that our approaches achieve competitive scores over the fully-supervised counterparts [17, 19, 31, 32] while with 2 \times to 5 \times fewer annotations. The strong augmentation and regularization ability of LaserMix further yields better results in high-data regime.

Qualitative examination. Fig. 5 visualizes the scene segmentation results for different SSL algorithms. We find that previous methods [26, 30, 13] can only improve predictions in limited regions, while our approaches can holistically eliminate false predictions in almost every direction around the ego-vehicle. The consistency enlightened by LaserMix has yielded better segmentation results compared to the baseline and prior arts.

3.3 Ablation Studies

Framework. The component analysis in Tab. 3 shows that \mathcal{L}_{mix} contributes significantly to the overall improvement. Meanwhile, using Teacher net instead of Student net to generate pseudo-labels leads to better results, as the formal is temporally ensembled and encourages consistency in-between mixed and original data, which is crucial besides enforcing confident predictions.

Mixing strategies. Fig. 4(a) compares LaserMix with other mixing methods [24, 33, 25]. MixUp and CutMix can be considered as setting A to random points and random areas, respectively. We observe that MixUp has no improvements over the baseline on average since there is no distribution pattern in random points. CutMix has a considerable improvement over the baseline, as there is always a structure prior in scene segmentation, *i.e.*, the same semantic class points tend to cluster, which reduces the entropy in any continuous area. This prior is often used in image semantic segmentation SSL [29]. However, our spatial prior is much stronger, where not only the area structure but also the area’s spatial position has been considered. LaserMix outperforms CutMix by a large margin (up to 3.3% mIoU) on all sets. CutOut can be considered as setting X_{out} to a dummy filling instead of sampling from datasets, and it leads to a considerable performance drop from CutMix.

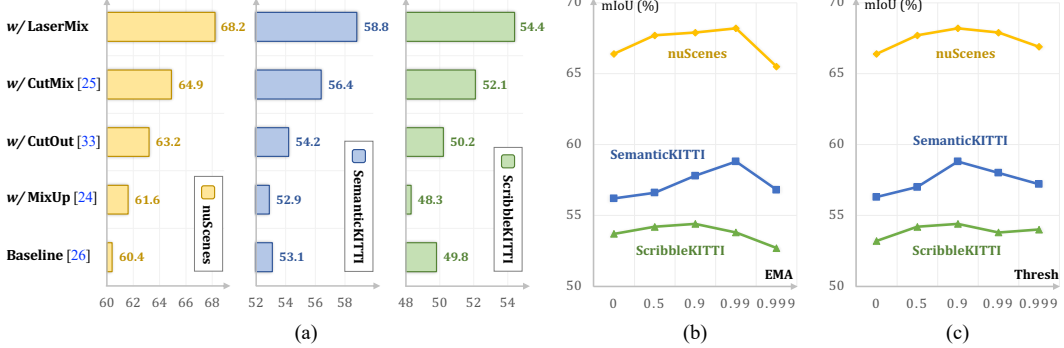


Figure 4: Ablation studies. **a)** Mixing techniques; **b)** EMA decay rate; **c)** Confidence threshold T .

Orderless mix. We revert the area ordering (*i.e.*, put the topmost laser beam at the bottom, and vice versa) in LaserMix, and the performance drops from 68.2% to 64.4% (-3.8% mIoU). When we shuffle the ordering, the performance drops to 63.8% (-4.4% mIoU), which becomes comparable with CutMix. In such cases, the spatial consistency is impaired, which highlights the importance of enforcing structural proper cues in LiDAR data. The results once again confirm the superiority of using spatial prior in LiDAR SSL.

Other heuristics. Besides our proposed inclination partition, the LiDAR scans can also be split based on azimuth (sensor horizontal direction). Results in Tab. 4 reveal that in contrast to laser partitioning, pure azimuth splitting (the first column) does not improve the performance, which is attributed to the fact that the semantic distribution has a weak correlation in the azimuth direction. We also observe that the results tend to improve as the mixing granularity increases (row direction in Tab. 4). The scores start to drop when the granularity is beyond a certain limit (*e.g.*, the last two columns). We conjecture that over-fine-grained partition and mixing tend to hurt semantic coherence. A trade-off between these two factors should be taken into consideration in order to maximize the gains.

Mix unlabeled data only. To verify that our method is more than trivially augmenting seen data and label pairs, we apply LaserMix only on unlabeled data. Instead of mixing an unlabeled scan with a labeled scan as described in Sec. 2.3, we mix two unlabeled scans with their pseudo-labels. The score drops from 68.2% to 66.9% (-1.3% mIoU) but still outperforms all existing methods by a large margin.

EMA. Fig. 4(b) provides results with different EMA decay rates. Typically, a rate between 0.9 and 0.99 yields the best possible results. Large rates like 0.999 tend to hurt the consistency between two networks. The results also verify that mean teacher [26] has good synergy with our proposed SSL framework. Thanks to our simplicity, more modern SSL techniques can be easily introduced in future works.

Confidence threshold. As pseudo-labels play an important role in our framework, we further analyze the impact of the threshold parameter T used in pseudo-label generation and show results in Fig. 4(c). When T is too low, a forced consistency to low-quality pseudo-labels tends to deteriorate the performance. When T is too high, the benefits from mixing might diminish. Generally, T is a dataset-dependent parameter and we find that a value around 0.9 leads to the best possible results on the three tested LiDAR segmentation sets in our benchmark.

Baseline	$(1\alpha, 2\phi)$	$(1\alpha, 3\phi)$	$(1\alpha, 4\phi)$	$(1\alpha, 5\phi)$	$(1\alpha, 6\phi)$
60.4	63.5 _(+3.1)	65.2 _(+4.8)	66.5 _(+6.1)	66.2 _(+5.8)	65.4 _(+5.0)
$(2\alpha, 1\phi)$	$(2\alpha, 2\phi)$	$(2\alpha, 3\phi)$	$(2\alpha, 4\phi)$	$(2\alpha, 5\phi)$	$(2\alpha, 6\phi)$
61.5 _(+1.1)	63.3 _(+2.9)	65.9 _(+5.5)	66.1 _(+5.7)	66.7 _(+6.3)	65.3 _(+4.9)
$(3\alpha, 1\phi)$	$(3\alpha, 2\phi)$	$(3\alpha, 3\phi)$	$(3\alpha, 4\phi)$	$(3\alpha, 5\phi)$	$(3\alpha, 6\phi)$
60.9 _(+0.6)	64.2 _(+3.8)	65.9 _(+5.5)	66.3 _(+5.9)	66.0 _(+5.6)	65.2 _(+4.8)
$(4\alpha, 1\phi)$	$(4\alpha, 2\phi)$	$(4\alpha, 3\phi)$	$(4\alpha, 4\phi)$	$(4\alpha, 5\phi)$	$(4\alpha, 6\phi)$
60.9 _(+0.6)	64.7 _(+4.3)	65.3 _(+4.9)	65.6 _(+5.2)	65.7 _(+5.3)	65.2 _(+4.8)

Table 4: Ablation on LiDAR partitions (horizontal: inclination ϕ ; vertical: azimuth α). $(i\alpha, j\phi)$ denotes that there are i azimuth and j inclination partitions.

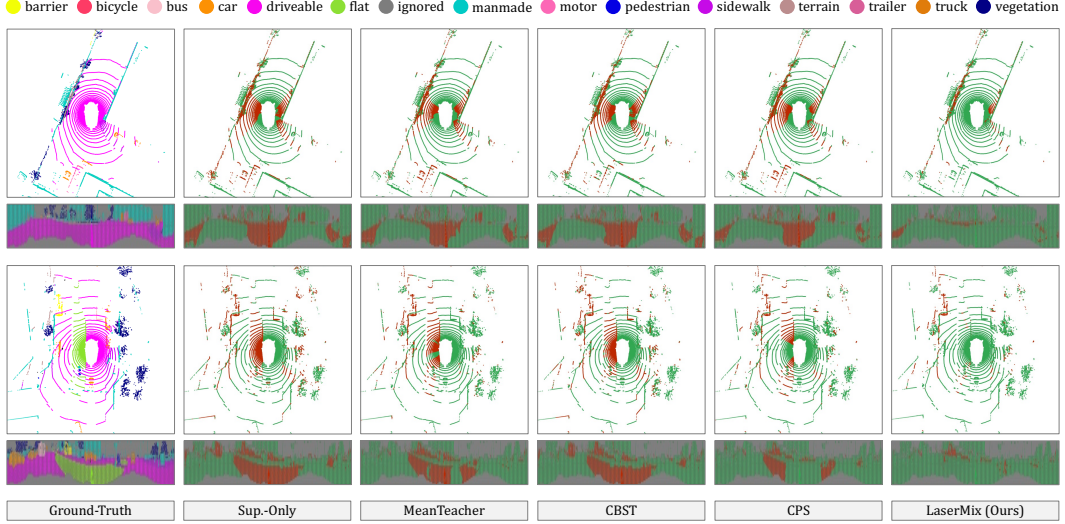


Figure 5: Qualitative results from LiDAR *top view* and *range view*. The **correct** and **incorrect** predictions are painted in **green** and **red** to highlight the difference. Best viewed in color.

4 Related Work

LiDAR segmentation. Various approaches from different aspects have been proposed for LiDAR scene segmentation, *i.e.*, range view [17, 34, 31, 21], bird’s eye view [19], voxel [35, 18, 36], and multi-view [37, 38] methods. Although appealing results have been achieved, these fully-supervised methods rely on large-scale annotated LiDAR datasets and their performance would degrade severely in the low-data regime [6]. Recent works seek weak [5, 39], scribble [4], and box [40] supervisions or activate learning [41, 42] to ease the annotation cost. We tackle this problem from the perspective of semi-supervised learning (SSL), aiming at directly leveraging the easy-to-acquire unlabeled data to boost LiDAR segmentation performance.

SSL in 2D. Well-known SSL algorithms are prevailing in handling image recognition problems [43, 26, 8, 10, 9]. In the context of semantic segmentation, CutMix-Seg [29] and PseudoSeg [44] apply perturbations on inputs and hope the decision boundary lies in the low-density region. CPS [13] and GCT [12] enforce consistency between two perturbed networks [45]. These perturbations [46, 47, 48], however, are either inapplicable or only yield sub-par results in 3D. Another line of research is entropy minimization. Methods like CBST [30] and ST++ [49] generate pseudo-labels [27] offline per round during self-training. The extra storage needed might become costly for large-scale LiDAR datasets [15, 16, 50]. Our framework encourages both consistency regularization and entropy minimization and does not require extra overhead, which better maintains scalability.

SSL in 3D. Most works focus on developing SSL for object-centric point clouds [51, 52] or indoor scenes [53, 54, 55], whose scale and diversity are much lower than the outdoor LiDAR point clouds [15, 16]. Some other works [56, 57, 58] try to utilize SSL for 3D object detection on LiDAR data. A recent work [14] tackles semi-supervised point cloud semantic segmentation using contrastive learning, but it still focuses on indoor scenes and does not distinguish between the uniformly distributed indoor point clouds and the spatially structured LiDAR point clouds. We are one of the first works to explore SSL for LiDAR segmentation. Our work also establishes a comprehensive benchmark upon popular autonomous driving databases [15, 16, 4].

5 Conclusion

In this work, we exploit the unique spatial prior in LiDAR point clouds for semi-supervised LiDAR semantic segmentation. We proposed a statistically-principled and effective SSL pipeline, including LaserMix, a novel LiDAR mixing technique that intertwines laser beams from different LiDAR scans. Through comprehensive empirical analysis, we show the importance of spatial prior and the superiority of our method on three popular LiDAR semantic segmentation datasets. The effectiveness

and simplicity of our framework have shed light on the scalable deployment of the LiDAR semantic mapping system. Our future work seeks to enhance more fine-grained spatial partitions and introduce more modern SSL techniques via our proposed framework.

Broader Impact: This work studies the important SSL problem for LiDAR semantic segmentation, which might be helpful to reduce both the time cost and human labor needed for annotating LiDAR point clouds in practice.

Limitation: Although we improve the LiDAR semantic segmentation performance in general, label bias and out-of-domain data are not addressed in this method, which could be safety-critical issues when deploying in the real-world autonomous driving applications.

6 Acknowledgment

We thank Fangzhou Hong for the insightful discussions and feedback.

Appendix

In this appendix, we provide the following content to support the findings and experimental results in the main body of this paper:

- Sec. 7 provides the technical details for the LiDAR range view and voxel representations.
- Sec. 8 gives a concrete case study on the strong spatial prior in the outdoor LiDAR data.
- Sec. 9 elaborates the implementation details for different SSL algorithms in our experiments.
- Sec. 10 provides additional experimental results.
- Sec. 11 acknowledges the public resources used during the course of this work.

7 LiDAR Representation

The LiDAR data has an unique and structural format. Various representations have been proposed to better capture the internal information in and between LiDAR points, including: raw points [59, 22, 20], range view (RV) [17, 21, 34, 31], bird’s eye view [19, 32], and voxel [18, 35] representations. This section reviews the technical details for RV projection and cylindrical voxel partition, which are currently the most efficient and the best-performing LiDAR representations, respectively.

7.1 Range View Projection

Given a LiDAR sensor with a fixed number (typically 32, 64, and 128) of laser beams and T times measurement in one scan cycle, we project LiDAR point (p^x, p^y, p^z) within this scan into a matrix $x_{\text{rv}}(u, v)$ (*i.e.*, range image) of size $h \times w$ via a mapping $\Pi : \mathbb{R}^3 \mapsto \mathbb{R}^2$, where h and w are the height and width, respectively. More concretely, this can be formulated as follows:

$$\begin{pmatrix} u \\ v \end{pmatrix} = \begin{pmatrix} \frac{1}{2} [1 - \arctan(p^y, p^x) \pi^{-1}] w \\ [1 - (\arcsin(p^z, r^{-1}) + \phi_{\text{up}}) \xi^{-1}] h \end{pmatrix}, \quad (11)$$

where (u, v) denotes the matrix grid coordinates of x_{rv} ; $r = \sqrt{(p^x)^2 + (p^y)^2 + (p^z)^2}$ is the range between the point and the LiDAR sensor; $\xi = |\phi_{\text{up}}| + |\phi_{\text{low}}|$ denotes the inclination range (also known as field-of-view or FOV) of the sensor; ϕ_{up} and ϕ_{low} are the inclinations at the upward direction and the downward direction, respectively.

Note that h is set based on the number of laser beams of the LiDAR sensor, and w is determined by its horizontal angular resolution. The projected range image $x_{\text{rv}}(u, v)$ serves as the input for RV-based LiDAR segmentation networks [17, 31, 21]. The semantic labels are projected in the same way as $x_{\text{rv}}(u, v)$.

For range view representation, training losses are calculated on the range view predictions of size $[k, h, w]$, where k denotes the number of semantic classes.

7.2 Cylindrical Partition

The cylinder voxels used in [18] exhibits better segmentation performance than the conventional cubic voxels on the LiDAR data. This is because the outdoor LiDAR point clouds have a varying density, which decreases as the range increases. More formally, the cylindrical partition transforms points in the Cartesian coordinate (p^x, p^y, p^z) into cylinder coordinate (ρ, α, p^z) , where ρ is the distance to the origin in X - Y plane and α is the azimuth in the sensor horizontal direction. The transformation can be formulated as follows:

$$\rho = \sqrt{(p^x)^2 + (p^y)^2}, \quad \alpha = \arctan\left(\frac{p^y}{p^x}\right). \quad (12)$$

Given a predefined voxel resolution $[n_\rho, n_\alpha, n_z]$, points in the cylinder coordinate can be partitioned into the corresponding voxel cells. The semantic labels are split into the partitioned cylinder voxels, where all points within the same voxel are assigned a unified label via majority voting.

For cylindircal representation, training losses are calculated on the voxel predictions of size $[k, n_\rho, n_\alpha, n_z]$, where k denotes the number of semantic classes.

8 Case Study: Spatial Prior in LiDAR Data

As mentioned in the main body of this paper, the LiDAR point clouds collected by the LiDAR sensor on top of the autonomous vehicle contain inherent spatial cues, which lead to strong patterns in laser beam partition. In this section, we conduct a case study on SemanticKITTI [16] to verify our findings (see Tab. 5).

8.1 Laser Partition

The LiDAR scans in the SemanticKITTI [16] dataset are collected by the Velodyne-HDLE64 sensor, which contains 64 laser beams emitted isotropically around the ego-vehicle with predefined inclination angles. In this study, we split each LiDAR point cloud into eight non-overlapping areas, *i.e.*, $A = \{a_1, a_2, \dots, a_8\}$. Each area a_i contains points captured from the consecutive 8 laser beams.

8.2 Spatial Prior

As can be seen from the fourth column in Tab. 5, different semantic classes have their own behaviors on these predefined areas. Specifically, the *road* class occupies mostly the first four areas (close to the ego-vehicle) while hardly appearing in the last two areas (far from the ego-vehicle). The *vegetation* class and the *building* class behavior conversely to *road* and appear at the long-distance areas (*e.g.*, a_6, a_7, a_8). The dynamic classes, including *car*, *bicyclist*, *motorcyclist*, and *person*, tend to appear in the middle-distance areas (*e.g.*, a_4, a_5, a_6). Similarly, from the heatmaps shown in the fifth column in Tab. 5, we can see that these semantic classes tend to appear (lighter colors) in only certain areas. For example, the *traffic-sign* class has a high likelihood to appear in the long-distance regions from the ego-vehicle (upper areas in the corresponding heatmap).

These unique distributions reflect the spatial layout of street scenes in real-world. In this work, we propose to leverage these strong spatial cues to construct our SSL framework. The experimental results verify that the spatial prior can better encourage consistency regularization in LiDAR segmentation under annotation scracity.

9 Implementation Details

In this section, we first compare the configuration details for the three LiDAR segmentation datasets (nuScenes [15], SemanticKITTI [16], and ScribbleKITTI [4]) used in this work (see Tab. 6). We then provide more detailed information on different SSL algorithms implemented in our semi-supervised LiDAR segmentation benchmark.

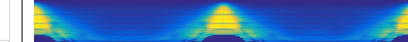
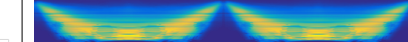
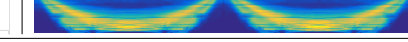
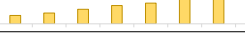
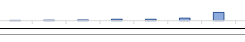
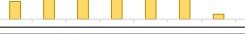
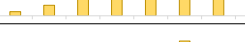
Class	Type	Proportion	Distribution	Heatmap
vegetation	static	24.825%		
road	static	22.545%		
sidewalk	static	16.353%		
building	static	12.118%		
terrain	static	8.122%		
fence	static	7.827%		
car	dynamic	4.657%		
parking	static	1.681%		
trunk	static	0.580%		
other-ground	static	0.396%		
pole	static	0.296%		
other-vehicle	dynamic	0.229%		
truck	dynamic	0.193%		
traffic-sign	static	0.061%		
motorcycle	dynamic	0.045%		
person	dynamic	0.036%		
bicycle	dynamic	0.018%		
bicyclist	dynamic	0.014%		
motorcyclist	dynamic	0.004%		

Table 5: A case study of the strong spatial prior in the LiDAR data (SemanticKITTI [16] in this example). For each semantic class, we show its type (static or dynamic), occupation (in percentage), distribution among eight areas ($A = \{a_1, a_2, \dots, a_8\}$), and heatmap in range view (lighter colors correspond to areas that have higher likelihood to appear and vice versa).

9.1 Data

nuScenes. As a comprehensive autonomous driving dataset, nuScenes³ [15] provides 1000 driving scenes of 20s duration each collected by a 32-beam LiDAR sensor from Boston and Singapore. We follow the official *train* and *val* sample splittings. The total number of LiDAR scans is 40000. The training and validation sets contain 28130 and 6019 scans, respectively. The semantic labels are annotated within the ranges: $p^x \in [50m, -50m]$, $p^y \in [50m, -50m]$, and $p^z \in [3m, -5m]$. Points outside the range are labeled as *ignored*. The inclination range is $[10^\circ, -30^\circ]$. We use the official label mapping which contains 16 semantic classes in total.

³Refer to the *lidarseg* set in nuScenes, details at: <https://www.nuscenes.org/lidar-segmentation>.

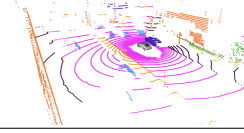
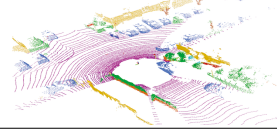
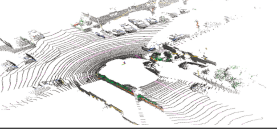
	nuScenes [15]	SemanticKITTI [16]	ScribbleKITTI [4]
Vis.			
#Class	16	19	19
#Train	29130	19130	19130
#Val	6019	4071	4071
Res. (RV)	32×1920	64×2048	64×2048
Res. (voxel)	[240, 180, 20]	[240, 180, 20]	[240, 180, 20]
#Beam	32	64	64
$[\phi_{\text{up}}, \phi_{\text{low}}]$	$[10^\circ, -30^\circ]$	$[3^\circ, -25^\circ]$	$[3^\circ, -25^\circ]$
$[p_x^{\text{max}}, p_x^{\text{min}}]$	[50m, -50m]	[50m, -50m]	[50m, -50m]
$[p_y^{\text{max}}, p_y^{\text{min}}]$	[50m, -50m]	[50m, -50m]	[50m, -50m]
$[p_z^{\text{max}}, p_z^{\text{min}}]$	[3m, -5m]	[2m, -4m]	[2m, -4m]
#Label	100%	100%	8.06%
Intensity			
Range			
Semantics			

Table 6: Configuration details for the three LiDAR segmentation datasets (nuScenes [15], SemanticKITTI [16], and ScribbleKITTI [4]) used in this work. Rows from top to bottom: visualization examples, number of semantic classes, number of training scans, number of validation scans, resolution for range view inputs, resolution for voxel inputs, number of laser beams, inclination angle range, x -axis range, y -axis range, z -axis range, the proportion of semantic labels, sensor intensity examples, range examples, and semantic label examples. Images in the second row are adopted from [50] and [4]. Images in the last three rows are generated from the corresponding datasets.

SemanticKITTI. Derived from the famous KITTI Vision Odometry Benchmark, SemanticKITTI [16] is another large-scale LiDAR segmentation dataset widely adopted in academia. It consists of 22 driving sequences, which are splitted into a *train* set (Seq. 00 to 10, where 08 is used for validation) and a *test* set (Seq. 11 to 21). The LiDAR point clouds are captured from Karlsruhe, Germany, by a 64-beam LiDAR sensor. The inclination range is $[3^\circ, -25^\circ]$. We follow the official label mapping and use 19 semantic classes in our experiments.

ScribbleKITTI. Efficiently annotating LiDAR point clouds is a viable solution for scaling up LiDAR segmentation. ScribbleKITTI [4] adopts scribbles to annotate SemanticKITTI [16], resulting in around 8.06% semantic labels compared to the dense annotations. The other configurations are the same as SemanticKITTI [16]. We use the densely annotated set (Seq. 08 in SemanticKITTI [16]) as the validation set.

In summary, we choose datasets with different number of laser beams (*i.e.*, 32 for nuScenes [15] and 64 for SemanticKITTI [16] and ScribbleKITTI [4]), different inclination ranges (*i.e.*, $[10^\circ, -30^\circ]$ for nuScenes [15] and $[3^\circ, -25^\circ]$ for SemanticKITTI [16] and ScribbleKITTI [4]), and different annotation proportions (*i.e.*, 100% for nuScenes [15] and SemanticKITTI [16] and 8.06% for ScribbleKITTI [4]). Our proposed SSL framework exhibit constant and evident improvements on all three datasets, which further verifies the scalability of our approaches.

9.2 Model Configurations

FIDNet. We use the *ResNet34-point* variant in FIDNet [21] as our *range view* segmentation backbone. It contains fewer parameters (6.05M) than the one used in the original paper (19.64M) while still maintaining good segmentation performance: 58.8% mIoU (compared to 59.5% mIoU) on the *val* set

of SemanticKITTI [16], and 71.6% mIoU (compared to 72.3% mIoU) on the *val* set of nuScenes [15]. We refer to the FIDNet [21] paper for more details on the model architecture.

Cylinder3D. We use a more compact version of Cylinder3D [18] as the *voxel* segmentation backbone in our experiments, which has 28.13M parameters (compared to 56.26M for the one used in the original paper). We also use a smaller voxel resolution ([240, 180, 20]) compared to the original configuration ([480, 360, 32]). This saves around 4 \times memory consumption and further helps to speed up training. We found that with the smaller resolution (larger voxel size), the performance drops from 76.1% mIoU to 74.1% mIoU on the *val* set of nuScenes [15]. We refer to the Cylinder3D [18] paper for more details on the model architecture.

Training configurations. All SSL algorithms implemented are sharing the same LiDAR segmentation backbones, *i.e.*, FIDNet [21] for the LiDAR *range view* representation and Cylinder3D [18] for the LiDAR *voxel* representation. For both FIDNet and Cylinder3D, we adopt AdamW [60] as the optimizer and use the OneCycle learning rate scheduler [61]. The maximum learning rate is 0.0025 for FIDNet and 0.001 for Cylinder3D. The batch size for the LiDAR *range view* representation is 10 for nuScenes and 4 for SemanticKITTI and ScribbleKITTI. The batch size for the LiDAR *voxel* representation is 8 for nuScenes and 4 for SemanticKITTI and ScribbleKITTI. All experiments can be conducted using a single NVIDIA Tesla V100 GPU with 32GB RAM.

Data augmentations. The data augmentations used for the *range view* inputs for all SSL algorithms include: random jittering, scaling, flipping (for nuScenes), and shifting (for SemanticKITTI and ScribbleKITTI). The data augmentations used for the *voxel* inputs for all SSL algorithms include: random rotation and flipping (for nuScenes, SemanticKITTI and ScribbleKITTI).

Other configurations. For LaserMix, the number of spatial areas is uniformly sampled from 1 to 6. The weight λ_{mix} is set as 1 for all three datasets. The weight λ_{mt} is set as 1e3 for nuScenes and 2e3 for SemanticKITTI and ScribbleKITTI. For CPS [13], the weight λ_{cps} is set as 1 for all three datasets. We tried 2 and 6 and found 1 yielded the best results. For MeanTeacher [26], the weight λ_{mt} is set as 1e3 for nuScenes and 2e3 for SemanticKITTI and ScribbleKITTI. For CutMix-Seg [29], the weight λ_{cons} is set as 1 which is the same as the original paper. For CBST [30], we use the *sup.-only* checkpoints to generate the pseudo-labels and then train the segmentation network from scratch with the pseudo-labels. We refer to the original papers for the aforementioned algorithms [13, 26, 29, 30] for other details.

10 Additional Experimental Results

In this section, we provide the class-wise IoU results for our comparative studies and ablation studies in the main body of this paper. Since our proposed SSL framework is a generic design, we also include the benchmarking results on Cityscapes [62] to further verify our generalizability on structural RGB data.

Comparative studies. Tab. 8, Tab. 9, and Tab. 10 provide the class-wise IoU scores for different SSL algorithms on the *val* set of nuScenes [15], SemanticKITTI [16], and ScribbleKITTI [4], respectively. For almost all semantic classes, we observe overt improvements from LaserMix. This can be credited to the strong consistency regularization encouraged by our SSL framework.

Ablation studies. Tab. 11 and Tab. 12 provide the class-wise IoU scores for the granularity studies of the LiDAR *range view* and *voxel* representations, respectively. Among different LaserMix strategies, we find that increasing the granularity along inclination tend to yield better segmentation performance. In our benchmarking experiments, we combine different strategies together by uniformly sampling the number of spatial areas. This simple ensembling further increases diversity and provides higher segmentation scores.

Extension to RGB data. To further attest the scalability of our proposed spatial-prior SSL framework, we conduct experiments on Cityscapes [62], which contains structural RGB images collected from

Method	1/16	1/8	1/4	1/2
MeanTeacher [26]	66.1	71.2	74.4	76.3
w/ Ours	68.7	72.3	75.7	76.8
$\Delta \uparrow$	+2.6	+1.1	+1.3	+0.5
CCT [11]	66.4	72.5	75.7	76.8
GCT [12]	65.8	71.3	75.3	77.1
CPS [13]	69.8	74.4	76.9	78.6
CPS-CutMix [13]	74.5	76.6	77.8	78.8
w/ Ours	75.5	77.1	78.3	79.1
$\Delta \uparrow$	+1.0	+0.5	+0.5	+0.3

Table 7: Benchmarking results on the *val* set of Cityscapes [62]. All mIoU scores are given in percentage (%).

street scenes. We follow the data split from recent work [13] and show the results in Tab. 7. Since the images from this dataset also contain strong spatial cues, the mixing strategy used here is similar to that for the LiDAR *range view* representation, *i.e.*, partitioning areas along the image vertical direction. We combine our proposed \mathcal{L}_{mix} with MeanTeacher [26] (\mathcal{L}_{mt}) and CPS [13] (\mathcal{L}_{cps}). The results verify that our SSL framework can also encourage consistency for image data. For all four splits, our approaches constantly improve the segmentation performance.

11 Public Resources Used

We acknowledge the use of the following public resources, during the course of this work:

- nuScenes⁴ CC BY-NC-SA 4.0
- nuScenes-devkit⁵ Apache License 2.0
- SemanticKITTI⁶ CC BY-NC-SA 4.0
- SemanticKITTI-API⁷ MIT License
- ScribbleKITTI⁸ Unknown
- FIDNet⁹ Unknown
- Cylinder3D¹⁰ Apache License 2.0
- TorchSemiSeg¹¹ MIT License
- MixUp¹² Attribution-NonCommercial 4.0 International
- CutMix¹³ MIT License
- CutMix-Seg¹⁴ MIT License
- CBST¹⁵ Attribution-NonCommercial 4.0 International
- MeanTeacher¹⁶ Attribution-NonCommercial 4.0 International
- Cityscapes¹⁷ Custom License by Daimler AG, MPI Informatics, TU Darmstadt

⁴<https://www.nuscenes.org/nuscenes>

⁵<https://github.com/nutonomy/nuscenes-devkit>

⁶<http://semantic-kitti.org>

⁷<https://github.com/PRBonn/semantic-kitti-api>

⁸<https://github.com/ouenal/scribblekitti>

⁹<https://github.com/placeforyiming/IROS21-FIDNet-SemanticKITTI>

¹⁰<https://github.com/xinge008/Cylinder3D>

¹¹<https://github.com/charlesCXK/TorchSemiSeg>

¹²<https://github.com/facebookresearch/mixup-cifar10>

¹³<https://github.com/clovaai/CutMix-PyTorch>

¹⁴<https://github.com/Britefury/cutmix-semisup-seg>

¹⁵<https://github.com/yzou2/CBST>

¹⁶<https://github.com/CuriousAI/mean-teacher>

¹⁷<https://www.cityscapes-dataset.com/>

Split	Repr.	Method	mIoU	barr	bicy	bus	car	const	moto	ped	cone	trail	truck	driv	othe	walk	terr	mann	veg
1%	Range View	Sup.-only	38.3	23.7	0.5	34.2	68.5	0.9	2.6	25.1	26.6	13.1	28.6	89.8	41.3	49.7	61.2	73.4	74.2
		MeanTeacher [26]	42.1	30.5	0.9	35.6	71.9	0.5	4.2	39.6	33.2	15.2	26.3	92.2	51.3	55.2	63.3	77.4	75.9
		CBST [30]	40.9	28.1	1.7	39.3	71.1	2.0	2.9	27.6	32.6	14.6	32.8	90.8	44.1	51.9	63.6	75.3	75.9
		CutMix-Seg [29]	43.8	44.6	0.7	30.8	75.7	0.4	2.7	36.9	38.1	18.1	29.8	92.5	45.9	56.9	67.6	80.1	80.0
		CPS [13]	40.7	28.4	0.4	38.3	73.5	0.3	0.5	36.1	25.4	13.6	22.4	91.5	44.1	54.4	66.1	77.8	78.8
		LaserMix	49.5	50.7	1.8	39.6	80.7	0.6	17.9	53.4	47.6	23.2	41.9	93.5	45.5	60.9	69.4	82.1	82.4
		Sup.-only	50.9	41.1	1.9	60.0	77.2	7.4	33.7	47.6	39.6	21.3	51.1	93.4	51.9	60.2	65.8	82.1	80.8
		MeanTeacher [26]	51.6	48.9	0.8	70.4	79.2	1.5	33.8	50.6	13.9	26.9	58.0	93.8	54.5	62.1	66.5	82.9	82.6
		CBST [30]	53.0	59.3	2.6	68.2	77.8	14.2	8.3	54.6	42.2	24.9	51.3	93.1	57.5	60.5	67.0	83.5	82.6
		CPS [13]	52.9	44.1	1.8	63.3	79.1	4.4	28.1	54.2	42.7	22.7	57.6	92.9	56.4	63.5	68.4	83.8	84.0
		LaserMix	55.3	53.6	1.9	67.2	79.2	21.1	29.7	57.3	46.8	28.0	55.5	93.6	54.8	62.1	66.5	83.9	83.3
	Voxel	Sup.-only	57.5	65.4	14.7	58.9	82.0	20.7	17.1	60.4	54.0	35.1	54.2	94.6	60.5	65.3	70.0	84.1	82.9
		MeanTeacher [26]	60.4	69.0	12.5	67.0	83.6	27.2	22.0	63.7	55.0	40.4	58.8	95.0	63.8	67.2	71.3	85.6	84.6
		CBST [30]	60.5	68.0	16.8	61.6	83.2	28.4	40.6	62.1	56.4	34.5	54.1	94.9	62.7	66.3	71.2	84.5	83.3
		CutMix-Seg [29]	63.9	70.5	22.7	69.2	83.4	26.6	69.5	65.2	54.7	39.4	59.2	95.2	68.3	72.3	84.3	82.8	82.8
		CPS [13]	60.8	66.6	9.8	66.6	85.7	22.4	19.7	63.5	57.2	43.4	62.2	95.4	65.3	69.8	73.8	85.9	85.3
		LaserMix	68.2	73.9	27.0	74.8	86.9	34.2	69.1	68.7	60.9	48.0	65.5	95.8	68.1	71.0	74.3	87.3	86.0
	10%	Sup.-only	65.9	69.5	14.0	87.2	83.5	30.8	61.9	63.5	55.7	47.6	75.2	95.1	63.5	68.1	69.6	85.8	84.1
		MeanTeacher [26]	66.0	71.1	19.7	85.1	83.3	42.0	43.5	64.0	54.9	45.6	73.7	95.3	66.8	69.8	69.6	86.7	84.9
		CBST [30]	66.5	70.1	13.6	85.9	82.2	35.1	59.1	61.9	52.1	57.5	74.0	94.5	65.0	70.1	71.8	86.6	85.0
		CPS [13]	66.3	72.3	16.4	84.5	81.8	38.5	60.3	62.7	53.4	47.1	70.1	94.7	65.4	70.1	71.7	87.1	85.5
		LaserMix	69.9	72.1	23.3	87.7	84.6	41.3	72.4	67.9	57.2	56.7	77.2	95.5	67.4	70.8	71.2	87.0	85.6
	20%	Sup.-only	62.7	69.4	19.1	69.7	84.9	29.1	36.4	64.0	58.5	44.6	61.0	95.2	63.6	67.2	70.9	85.7	84.6
		MeanTeacher [26]	65.4	70.7	18.9	75.3	85.6	32.4	48.5	72.2	59.0	46.1	64.0	95.2	65.3	68.3	72.8	86.9	85.7
		CBST [30]	64.3	71.6	19.0	70.4	84.4	29.9	49.7	66.2	60.8	46.3	61.3	95.4	62.3	68.4	71.7	86.1	84.6
		CutMix-Seg [29]	64.8	72.7	23.2	71.8	86.3	34.3	38.2	69.4	59.1	46.9	63.2	95.5	62.0	69.1	72.7	86.9	85.6
		CPS [13]	64.9	69.6	7.0	75.1	86.6	23.5	50.8	68.5	59.0	50.2	66.5	95.8	68.8	71.1	73.9	85.9	85.6
		LaserMix	70.6	74.1	26.1	80.3	89.2	36.2	74.6	73.1	62.8	55.0	73.4	96.0	68.6	71.3	74.3	88.1	86.7
	20%	Sup.-only	66.6	71.5	27.1	82.1	82.7	37.2	68.6	63.6	53.4	42.2	70.5	94.8	65.9	67.8	69.4	85.1	83.7
		MeanTeacher [26]	67.1	72.1	26.0	89.1	84.4	39.5	18.4	71.3	57.6	59.3	77.5	95.6	66.9	71.3	71.9	87.6	85.8
		CBST [30]	69.6	73.4	29.5	86.1	83.7	37.0	75.7	66.7	56.6	53.0	73.7	95.5	68.5	71.5	70.8	87.3	85.6
		CPS [13]	70.0	73.1	29.3	88.0	83.4	37.2	76.0	66.6	57.8	54.5	75.7	95.5	67.8	71.2	70.5	87.4	85.9
		LaserMix	71.8	73.6	32.1	89.6	84.1	41.4	77.0	69.0	60.0	60.9	78.7	95.8	69.6	72.2	72.9	87.9	84.5
	50%	Sup.-only	67.6	72.5	32.6	78.5	87.4	32.8	43.6	70.6	62.3	54.0	68.3	95.7	66.4	69.8	72.7	87.7	86.4
		MeanTeacher [26]	69.4	73.4	33.0	81.2	87.6	35.2	61.0	71.9	62.3	55.1	69.4	95.8	66.5	71.1	73.1	87.5	86.1
		CBST [30]	69.3	72.7	35.2	80.8	88.0	35.7	53.7	68.2	62.9	60.2	72.0	95.5	67.4	70.3	73.0	87.3	85.8
		CutMix-Seg [29]	69.8	74.4	33.5	79.9	88.7	37.3	60.8	70.9	62.0	57.8	70.6	95.8	67.3	70.9	73.3	87.5	85.8
		CPS [13]	68.0	71.2	31.8	71.9	87.1	29.0	57.4	67.4	62.3	58.6	69.0	95.6	68.7	71.1	74.1	86.7	85.4
		LaserMix	73.0	76.0	35.6	85.0	89.9	43.3	76.6	72.5	63.9	61.5	75.1	96.1	69.6	72.3	74.8	88.2	86.9
	Voxel	Sup.-only	71.2	73.1	35.6	89.0	85.2	41.2	73.3	67.9	59.2	50.9	78.4	95.6	71.5	72.0	73.0	87.3	85.9
		MeanTeacher [26]	71.7	73.7	36.2	90.6	85.0	42.3	76.5	68.3	54.9	61.4	74.3	95.7	69.9	72.2	72.6	87.2	86.0
		CBST [30]	71.6	73.3	36.1	90.2	84.8	42.2	75.7	67.8	56.6	61.5	74.3	95.7	69.1	72.2	72.7	87.1	85.9
		CPS [13]	72.5	73.9	35.6	91.0	84.9	42.9	79.0	68.6	60.3	60.1	78.3	95.8	71.2	72.3	73.2	87.6	85.2
		LaserMix	73.2	74.5	36.3	91.1	84.9	48.2	78.5	70.5	59.6	59.8	78.9	95.1	70.7	73.5	74.1	88.6	86.9

Table 8: Class-wise IoU scores for different SSL algorithms on the *val* set of nuScenes [15]. All IoU scores are given in percentage. The *sup.-only* and the *best* scores for each semantic class within each split are highlighted in **red** and **blue**, respectively.

Split	Repr.	Method	mIoU	car	bicy	moto	truck	bus	ped	b.cyc	m.cyc	road	park	walk	o.gro	build	fence	veg	trunk	terr	pole	sign
1%	Range View	Sup.-only	36.2	86.8	0.6	0.0	13.0	5.7	12.1	6.6	0.0	87.9	13.4	71.3	0.1	80.4	42.3	78.7	38.1	62.8	52.5	35.7
		MeanTeacher [26]	37.5	88.0	0.1	0.1	12.4	3.6	13.0	12.6	0.0	89.2	19.6	73.0	0.0	81.6	44.8	80.2	41.8	64.4	54.0	33.3
		CBST [30]	39.9	89.4	1.9	0.0	4.6	5.8	27.3	3.4	0.0	91.3	25.9	76.5	0.0	83.9	49.1	82.7	56.4	68.1	57.5	33.6
		CutMix-Seg [29]	37.4	86.6	0.2	0.0	3.2	1.5	18.6	6.4	0.0	90.8	24.2	74.9	0.0	81.5	45.5	81.3	50.0	65.7	52.9	34.6
		CPS [13]	36.5	88.9	0.0	0.0	3.1	0.4	5.7	2.7	0.0	90.8	13.7	76.7	0.0	83.4	52.2	79.9	40.8	63.8	55.9	32.3
	Voxel	LaserMix	43.4	88.8	37.1	0.2	2.1	4.1	10.7	40.7	0.2	91.9	32.3	77.0	0.0	83.9	48.8	81.4	55.9	69.4	59.0	41.7
		Sup.-only	45.4	90.9	24.5	2.8	35.1	20.4	31.7	49.5	0.0	85.5	23.4	67.5	1.3	85.0	46.0	84.1	49.1	70.3	55.0	40.6
		MeanTeacher [26]	45.4	91.2	13.2	5.4	47.3	14.5	29.0	37.3	0.0	86.8	22.6	70.3	1.2	86.7	45.4	84.7	59.4	70.9	55.8	40.8
		CBST [30]	48.8	92.4	16.3	6.4	61.9	27.0	35.7	49.4	0.0	88.9	29.4	73.2	0.7	89.1	49.5	83.9	51.4	68.1	59.8	44.0
		CPS [13]	46.7	92.0	13.5	7.1	37.8	12.7	33.0	54.5	0.0	89.8	25.0	73.8	0.4	88.8	50.1	83.6	57.4	67.8	58.2	42.1
	10%	LaserMix	50.6	91.8	35.7	19.8	37.5	25.6	53.6	45.7	2.5	87.8	33.5	71.3	0.7	87.3	43.8	84.6	62.7	69.3	59.8	47.6
		Sup.-only	52.2	90.4	34.2	22.6	48.2	24.5	59.7	60.9	0.0	92.2	31.8	78.1	0.5	85.7	47.9	83.9	59.3	69.3	59.0	44.2
		MeanTeacher [26]	53.1	91.1	30.8	23.1	58.9	27.5	60.1	57.9	0.0	92.9	34.7	78.7	0.9	87.3	53.5	83.3	59.6	66.9	57.0	44.1
		CBST [30]	53.4	91.7	33.7	28.9	62.0	29.7	57.9	55.2	0.0	92.9	32.5	78.7	0.8	87.1	53.7	83.5	59.4	68.1	56.7	42.4
		CutMix-Seg [29]	54.3	90.9	34.9	37.2	57.4	31.7	56.1	63.9	0.0	92.9	34.5	78.6	0.5	87.0	52.3	83.6	58.8	65.2	44.7	
		CPS [13]	52.3	90.2	32.8	19.7	54.0	23.8	56.8	50.5	0.0	92.7	36.3	79.5	0.4	87.6	52.0	85.7	59.4	69.2	58.6	45.1
		LaserMix	58.8	92.0	43.5	50.4	76.1	37.1	69.9	74.3	0.0	93.4	38.8	80.1	0.6	87.1	53.3	84.2	63.2	68.3	58.8	45.3
		Sup.-only	56.1	93.4	38.4	47.7	65.7	31.0	61.9	64.9	0.0	90.7	37.7	75.3	0.9	89.2	50.5	86.4	56.0	73.9	56.2	46.0
		MeanTeacher [26]	57.1	94.1	40.5	58.4	56.0	38.0	66.5	75.6	0.0	88.4	22.7	72.0	1.5	87.9	49.3	86.7	66.1	74.2	58.0	49.2
		CBST [30]	58.3	93.6	40.3	43.5	80.4	33.8	57.6	78.1	0.0	91.6	36.3	76.6	5.1	89.2	51.1	86.3	61.9	71.2	61.3	49.7
	20%	CPS [13]	58.7	94.0	38.7	51.0	60.3	39.8	65.7	80.0	0.0	91.4	33.2	76.4	2.9	89.8	53.8	87.2	65.7	74.6	61.5	50.0
		LaserMix	60.0	93.8	44.9	58.4	65.6	39.4	65.8	80.9	0.2	92.0	44.2	77.1	3.9	89.1	49.0	86.2	66.8	72.3	58.4	51.2
		Sup.-only	55.9	92.2	38.4	34.9	68.8	35.1	63.1	69.4	0.0	93.1	33.8	79.0	1.1	86.6	50.4	84.1	60.9	69.2	56.9	45.3
		MeanTeacher [26]	56.1	93.2	33.1	36.3	67.3	39.1	64.9	66.8	0.0	93.3	36.7	79.8	1.0	87.6	54.0	83.9	60.7	67.7	56.5	43.7
		CBST [30]	56.1	92.8	33.2	33.9	64.9	38.9	66.6	69.1	0.0	93.2	36.9	79.7	1.7	87.3	53.6	84.5	60.7	69.1	55.1	44.9
		CutMix-Seg [29]	56.6	91.5	42.8	39.8	60.6	32.9	64.3	71.6	0.0	93.1	39.8	79.3	0.6	87.1	53.8	85.0	61.6	71.0	56.1	45.4
		CPS [13]	56.3	90.8	44.0	40.7	67.9	30.7	65.5	58.0	0.0	93.3	39.1	79.5	1.1	87.5	55.6	83.8	60.4	67.9	56.8	46.7
	50%	LaserMix	59.4	92.5	43.3	51.5	73.1	45.8	69.4	74.7	0.0	94.0	40.4	80.4	5.0	87.3	53.7	83.8	64.1	66.7	58.0	44.6
		Sup.-only	57.8	94.0	31.6	47.3	89.5	38.3	57.9	79.1	0.0	91.6	29.6	76.1	0.9	87.8	43.6	86.6	63.7	72.5	61.8	47.5
		MeanTeacher [26]	59.2	94.4	38.7	52.5	81.2	45.8	64.2	78.0	0.0	90.9	35.2	75.7	1.8	89.2	49.8	86.3	65.6	72.6	56.0	47.6
		CBST [30]	59.4	94.2	41.8	51.4	77.7	39.8	65.4	79.8	0.0	91.7	29.8	76.3	3.5	89.2	49.7	87.1	66.1	74.2	60.1	51.3
		CPS [13]	59.6	94.2	41.8	52.9	78.2	39.6	66.1	80.6	0.0	91.9	30.2	76.4	3.7	89.2	50.0	87.0	66.6	73.7	60.0	51.1
		LaserMix	61.9	94.4	46.0	68.0	74.3	47.6	68.1	83.7	0.2	92.6	42.7	78.0	1.9	89.7	52.9	86.0	69.3	70.6	59.2	51.7
		Sup.-only	57.2	91.3	41.1	47.7	70.2	41.2	66.0	74.4	0.0	93.0	39.2	79.2	2.0	86.0	44.2	83.4	59.3	68.6	55.5	45.1
		MeanTeacher [26]	57.4	93.1	38.6	42.4	61.0	45.0	65.7	73.9	0.0	93.1	38.1	79.4	2.1	87.5	53.8	85.0	60.3	71.5	53.6	47.2
		CBST [30]	56.9	91.5	40.0	42.9	66.1	41.7	64.8	74.2	0.0	93.0	34.9	79.2	1.2	87.0	48.7	83.7	59.6	68.9	55.3	47.1
		CutMix-Seg [29]	57.6	92.0	43.3	48.9	44.6	40.7	67.4	78.5	0.0	93.3	39.1	79.7	3.0	87.2	54.2	86.0	61.6	74.8	55.1	44.8
	Voxel	CPS [13]	57.4	92.1	38.5	44.3	69.6	45.2	66.5	71.0	0.0	93.5	36.6	80.1	1.7	87.0	48.0	83.9	62.3	68.0	58.0	43.7
		LaserMix	61.4	92.5	45.6	58.8	73.0	53.2	71.2	82.4	0.0	93.7	43.2	80.7	5.5	87.5	52.6	85.4	64.0	71.9	57.9	47.9
		Sup.-only	58.7	93.9	40.4	48.0	81.4	33.7	65.7	79.7	0.0	91.9	32.6	76.7	1.3	89.0	51.8	87.2	61.4	72.5	58.7	48.7
		MeanTeacher [26]	60.0	94.1	41.3	57.7	64.6	39.5	65.3	86.8	0.0	91.3	32.8	75.2	3.5	89.7	48.6	85.4	65.9	70.6	58.7	49.1
		CBST [30]	59.7	94.9	40.9	54.4	75.3	43.8	67.3	86.8	0.0	91.5	33.3	75.7	2.6	89.3	50.7	86.7	63.9	72.4	56.4	48.8
		CPS [13]	60.5	94.6	43.3	55.3	80.5	42.5	67.9	84.6	0.0	92.0	34.3	76.9	2.2	89.8	52.3	86.0	67.4	71.1	59.5	49.4
		LaserMix	62.3	94.7	48.4	64.7	65.2	44.5	71.0	88.3	2.1	92.7	43.0	78.4	2.0	90.3	54.9	88.1	68.1	75.3	66.6	51.7

Table 9: Class-wise IoU scores for different SSL algorithms on the *val* set of SemanticKITTI [16]. All IoU scores are given in percentage. The **sup.-only** and the **best** scores for each semantic class within each split are highlighted in **red** and **blue**, respectively.

Split	Repr.	Method	mIoU	car	bicy	moto	truck	bus	ped	b.cyc	m.cyc	road	park	walk	o.gro	build	fence	veg	trunk	terr	pole	sign
1%	Range View	<i>Sup.-only</i>	33.1	81.3	2.6	0.4	11.7	8.3	11.5	8.7	0.0	76.7	10.9	61.8	0.1	75.8	26.3	73.8	40.7	56.1	48.9	32.5
		MeanTeacher [26]	34.2	82.3	1.7	0.1	10.4	6.7	6.1	4.7	0.0	78.6	13.4	67.8	0.1	80.7	31.3	76.1	43.1	60.0	53.3	32.8
		CBST [30]	35.7	84.8	1.6	0.4	11.7	10.6	14.9	8.0	0.0	83.6	13.4	68.1	0.1	79.5	32.4	77.1	44.6	60.5	53.0	34.4
		CutMix-Seg [29]	36.7	84.7	0.9	0.0	5.5	0.9	18.7	1.9	0.0	89.3	25.1	74.6	0.1	82.6	27.0	77.7	52.1	65.0	54.7	35.8
		CPS [13]	33.7	82.7	0.1	0.0	0.9	0.1	2.9	4.1	0.0	85.9	8.9	70.8	0.0	81.2	47.3	78.1	36.0	61.2	51.9	27.5
	Voxel	LaserMix	38.3	86.5	1.9	0.9	12.8	2.9	25.9	2.6	0.0	90.8	25.0	75.8	1.0	83.9	26.4	77.8	55.5	63.9	56.7	38.2
		<i>Sup.-only</i>	39.2	83.2	13.8	3.4	26.3	11.8	28.0	25.2	0.0	72.5	13.0	59.5	0.2	86.6	33.7	78.7	55.7	58.4	54.0	40.3
		MeanTeacher [26]	41.0	82.3	15.8	7.1	32.0	15.4	23.7	36.3	0.0	75.0	12.6	61.4	0.9	85.3	30.0	80.1	57.0	67.0	56.1	41.3
		CBST [30]	41.5	83.7	22.1	5.9	28.3	13.4	27.1	34.7	0.0	74.0	14.4	61.7	0.2	88.1	36.6	80.3	58.7	60.4	57.1	41.4
		CPS [13]	41.4	82.8	18.2	11.4	20.9	15.1	22.5	35.5	0.0	74.7	15.7	61.6	0.4	86.0	34.2	82.2	58.4	69.9	56.7	40.0
	10%	LaserMix	44.2	82.6	25.5	18.8	29.0	19.8	41.1	47.2	0.6	71.5	10.5	64.2	2.2	85.1	33.5	82.0	59.9	65.8	54.5	45.2
		<i>Sup.-only</i>	47.7	85.1	30.2	20.4	40.4	20.9	54.4	55.9	0.0	82.8	21.6	68.4	0.5	84.2	40.5	80.3	58.6	61.9	56.0	45.2
		MeanTeacher [26]	49.8	83.5	30.0	22.7	62.2	31.1	59.1	52.4	0.0	77.9	17.6	70.5	2.0	86.8	42.6	82.0	61.2	62.6	58.4	46.5
		CBST [30]	50.7	90.3	27.2	18.1	53.1	24.6	60.3	56.5	0.0	90.3	32.4	76.0	0.7	86.1	46.0	81.1	58.7	64.5	51.7	45.0
		CutMix-Seg [29]	50.7	87.4	28.1	25.9	60.5	24.5	58.4	57.7	0.0	85.5	27.5	72.1	1.3	84.7	39.4	82.4	58.8	68.3	56.4	44.4
		CPS [13]	50.0	85.8	26.7	17.4	54.5	20.5	54.4	53.7	0.0	88.9	29.2	74.4	0.6	86.5	48.6	82.4	58.6	65.2	57.3	45.1
		LaserMix	54.4	87.1	35.4	44.4	62.5	36.4	66.9	72.6	0.0	80.8	27.8	73.7	0.6	85.2	35.2	83.9	60.6	70.0	59.3	51.6
		<i>Sup.-only</i>	48.0	85.7	25.6	21.3	52.8	29.9	46.5	47.2	0.1	79.5	15.4	63.8	0.3	85.4	39.6	84.8	59.7	71.5	57.7	45.8
		MeanTeacher [26]	50.1	83.7	32.6	45.1	41.0	34.7	56.0	59.2	0.0	75.9	14.0	64.0	0.7	85.6	37.9	83.3	62.6	68.2	59.7	47.0
		CBST [30]	50.6	85.8	31.4	30.5	58.5	24.4	55.1	58.8	0.0	82.6	15.3	67.8	0.5	88.7	40.0	82.8	62.5	65.0	62.0	50.8
	20%	LaserMix	51.8	84.6	34.9	47.1	37.5	29.5	60.1	69.1	0.0	79.8	16.5	67.3	2.7	88.0	39.2	84.5	64.5	71.0	60.4	47.9
		<i>Sup.-only</i>	53.7	85.8	34.7	45.6	54.9	35.8	63.2	73.6	1.3	79.8	25.0	68.2	1.8	87.7	35.4	84.0	65.8	70.8	59.4	48.2
		<i>Sup.-only</i>	49.9	86.3	32.2	23.8	49.5	30.3	60.5	58.4	0.0	83.6	22.4	69.5	1.1	85.1	40.6	80.9	59.9	62.3	55.9	46.4
		MeanTeacher [26]	51.6	82.9	27.7	43.1	59.5	32.8	59.5	60.7	0.0	80.8	25.7	70.3	0.7	85.3	41.6	82.1	60.5	66.0	55.6	45.7
		CBST [30]	52.7	90.0	33.1	30.2	53.6	33.8	60.0	60.4	0.0	89.3	30.3	75.8	0.6	85.6	44.8	83.5	58.6	70.3	54.7	47.1
		CutMix-Seg [29]	52.9	86.9	30.0	35.6	64.8	35.7	60.9	63.6	0.0	88.3	29.0	74.7	0.9	85.2	40.3	82.0	59.4	65.2	56.5	45.5
		CPS [13]	52.8	86.3	35.4	28.1	67.1	27.7	59.5	59.2	0.0	89.0	28.0	75.0	0.8	86.7	47.3	83.1	61.0	66.9	58.1	44.6
	50%	LaserMix	55.6	87.3	36.0	34.3	69.5	40.6	66.3	70.6	0.0	84.2	27.2	72.3	2.4	86.4	44.6	84.1	62.8	69.8	59.4	57.7
		<i>Sup.-only</i>	52.1	86.9	38.0	39.5	67.3	29.7	56.5	69.9	0.0	79.0	16.0	66.0	0.3	87.0	38.6	84.3	60.6	66.2	58.8	45.2
		MeanTeacher [26]	52.8	85.9	27.9	41.5	55.5	33.0	64.1	72.0	1.2	81.0	22.5	67.8	1.2	89.1	39.9	82.9	63.7	66.9	60.5	46.7
		CBST [30]	53.3	86.6	36.8	40.9	72.9	28.3	58.0	69.5	0.0	81.1	18.3	68.2	0.7	88.7	44.3	83.6	63.3	64.4	60.3	47.5
		CPS [13]	53.9	85.4	37.2	44.7	58.9	32.9	63.5	71.0	0.0	81.6	23.1	69.2	1.9	88.4	38.2	83.8	65.7	69.2	60.2	48.9
	Voxel	LaserMix	55.1	88.0	38.8	51.3	54.8	36.6	60.2	73.9	0.0	78.8	22.7	71.9	1.5	90.3	43.3	85.3	66.5	70.9	60.3	51.6
		<i>Sup.-only</i>	52.5	86.7	35.9	40.2	55.9	30.1	63.2	62.9	0.1	83.6	25.3	70.8	1.1	85.1	40.0	82.9	60.4	69.0	56.3	48.3
		MeanTeacher [26]	53.3	86.9	31.9	37.5	58.6	36.3	63.3	62.0	0.0	87.6	29.5	74.1	1.0	86.4	40.7	82.6	61.3	68.9	58.0	47.0
		CBST [30]	54.6	90.1	36.0	36.6	64.7	41.6	61.2	66.7	0.0	90.4	33.8	76.8	3.8	84.5	44.3	83.7	57.6	70.2	48.4	47.8
		CutMix-Seg [29]	54.3	88.1	35.3	40.0	68.8	39.3	62.4	69.8	0.0	88.0	32.0	74.3	0.9	85.1	38.4	82.4	59.3	67.4	56.3	44.5
		CPS [13]	54.6	87.1	35.0	41.0	66.1	40.8	63.2	65.5	0.0	87.9	30.0	74.6	1.4	86.1	42.4	82.7	60.9	67.9	57.5	48.2
		LaserMix	58.7	88.2	37.1	56.0	80.9	51.8	70.8	75.0	0.0	87.0	31.8	74.7	0.8	86.6	41.3	84.6	62.1	72.9	59.8	53.7
		<i>Sup.-only</i>	53.8	87.5	37.2	41.3	71.4	29.6	58.8	80.4	0.0	81.1	16.7	67.5	0.4	88.4	39.4	83.1	64.4	65.5	61.8	47.5
		MeanTeacher [26]	53.9	86.9	33.6	46.2	48.9	33.2	62.8	77.7	0.0	82.7	22.8	68.6	3.2	89.2	38.6	83.8	66.4	68.0	62.3	48.5
		CBST [30]	54.5	87.6	39.5	36.7	65.9	35.7	62.8	78.1	0.0	82.4	20.4	69.6	0.1	88.8	42.3	84.2	64.0	67.4	60.1	50.1
		CPS [13]	54.8	85.1	35.2	45.2	68.6	32.0	65.7	77.9	0.2	81.2	21.7	69.0	1.6	89.2	40.2	84.5	65.1	70.1	60.9	48.5

Table 10: Class-wise IoU scores for different SSL algorithms on the *val* set of ScribbleKITTI [4] (the same as SemanticKITTI [16]). All IoU scores are given in percentage. The *sup.-only* and the **best** scores for each semantic class within each split are highlighted in red and blue, respectively.

Method	Illustr.	mIoU	barr	bicy	bus	car	const	moto	ped	cone	trail	truck	driv	othe	walk	terr	mann	veg
Baseline		60.4	69.0	12.5	67.0	83.6	27.2	22.0	63.7	55.0	40.4	58.8	95.0	63.8	67.2	71.3	85.6	84.6
$(1\alpha, 2\phi)$		63.5	70.8	17.8	65.3	84.9	26.9	44.7	65.8	59.2	46.6	62.2	95.5	64.3	69.2	72.5	86.1	84.9
$(1\alpha, 3\phi)$		65.2	72.3	21.5	67.1	85.1	26.2	57.1	70.4	59.3	45.8	60.7	95.6	65.4	69.3	73.7	87.0	85.9
$(1\alpha, 4\phi)$		66.5	73.7	22.4	72.9	87.0	26.3	59.4	70.2	60.3	44.7	64.7	95.8	67.8	70.9	74.2	87.0	85.9
$(1\alpha, 5\phi)$		66.2	72.8	24.1	74.0	85.7	36.3	47.8	71.5	60.8	45.8	64.5	95.7	64.8	69.9	73.3	87.1	85.9
$(1\alpha, 6\phi)$		65.4	72.6	25.2	69.8	84.6	33.8	48.3	70.1	60.5	44.8	61.9	95.4	65.3	68.9	73.3	86.8	85.5
$(2\alpha, 1\phi)$		61.5	68.4	19.1	67.1	83.5	28.1	26.1	64.8	57.6	41.5	59.0	95.1	64.4	68.1	72.0	85.4	84.3
$(2\alpha, 2\phi)$		63.3	70.8	11.9	64.8	84.4	27.3	51.4	69.2	58.3	41.8	59.5	95.6	63.8	69.8	73.2	86.2	85.3
$(2\alpha, 3\phi)$		65.9	71.9	24.2	69.1	86.3	28.2	58.5	71.5	60.1	44.7	63.4	95.7	65.3	70.1	73.4	86.9	85.9
$(2\alpha, 4\phi)$		66.1	72.9	27.8	70.4	86.4	34.2	54.1	71.4	61.5	42.9	61.3	95.4	64.6	69.0	73.3	86.9	85.8
$(2\alpha, 5\phi)$		66.7	73.1	20.5	69.6	87.5	27.1	67.8	71.1	61.0	43.4	64.6	95.6	69.1	70.1	74.1	87.0	85.7
$(2\alpha, 6\phi)$		65.3	71.9	23.5	68.6	85.3	32.2	51.0	69.6	60.2	45.2	63.6	95.4	63.6	69.2	73.3	86.4	85.1
$(3\alpha, 1\phi)$		60.9	67.4	14.7	65.3	82.9	25.2	39.5	63.6	57.0	34.7	55.2	95.0	64.6	67.1	71.4	85.6	84.7
$(3\alpha, 2\phi)$		64.2	71.4	15.5	66.3	86.2	25.8	54.4	68.4	60.4	44.3	63.2	95.5	63.3	69.3	72.6	86.3	85.1
$(3\alpha, 3\phi)$		65.9	73.1	15.7	74.4	85.3	28.0	59.7	69.0	60.6	45.3	63.4	95.6	68.8	70.5	74.3	86.5	85.2
$(3\alpha, 4\phi)$		66.3	72.1	16.7	73.1	86.2	34.2	66.6	67.3	58.4	45.5	62.4	95.7	65.6	70.5	74.0	86.7	85.6
$(3\alpha, 5\phi)$		66.0	72.1	18.4	72.7	86.0	31.9	68.8	66.0	58.3	42.9	61.9	95.6	65.7	70.0	73.9	86.5	85.4
$(3\alpha, 6\phi)$		65.2	71.0	26.4	68.6	85.6	29.3	54.7	69.1	59.6	43.5	62.1	95.3	63.9	68.7	73.4	86.3	85.1
$(4\alpha, 1\phi)$		60.9	69.1	16.7	66.2	83.7	23.5	26.8	64.4	56.2	40.6	60.4	95.0	63.7	67.0	71.5	85.6	84.6
$(4\alpha, 2\phi)$		64.7	71.0	16.7	66.4	84.7	28.4	59.4	70.6	60.7	42.1	60.3	95.4	65.4	69.6	73.2	86.4	85.5
$(4\alpha, 3\phi)$		65.3	72.0	24.9	68.5	85.6	25.1	52.7	71.3	59.3	45.2	62.3	95.5	66.9	69.6	73.1	86.8	85.8
$(4\alpha, 4\phi)$		65.6	71.9	21.3	71.3	86.4	32.8	44.0	69.3	61.8	45.5	64.0	95.7	67.7	70.2	73.9	87.1	86.2
$(4\alpha, 5\phi)$		65.7	71.9	24.8	72.1	84.5	31.6	52.2	71.6	60.6	43.6	60.4	95.5	65.1	70.1	73.8	87.1	86.1
$(4\alpha, 6\phi)$		65.2	72.1	18.8	69.9	83.7	32.5	57.2	69.0	60.2	43.2	59.1	95.5	66.1	69.8	73.5	87.0	86.1

Table 11: Class-wise IoU scores for granularity studies on the *range view* representation (under 10% split on the *val* set of nuScenes [15]). All scores are given in percentage. The best score for each semantic class is highlighted in **bold**.

Method	Illustr.	mIoU	barr	bicy	bus	car	const	moto	ped	cone	trail	truck	driv	othe	walk	terr	mann	veg
Baseline		66.0	71.1	19.7	85.1	83.3	42.0	43.5	64.0	54.9	45.6	73.7	95.3	66.8	69.8	69.6	86.7	84.9
$(1\alpha, 2\phi)$		68.7	72.4	20.7	87.0	83.1	38.3	66.7	65.8	57.5	54.9	76.6	95.4	67.1	70.3	71.6	86.9	84.6
$(1\alpha, 3\phi)$		69.0	71.5	21.5	87.0	83.7	39.5	68.1	66.1	57.5	56.6	77.2	95.5	66.5	70.7	71.9	86.9	84.6
$(1\alpha, 4\phi)$		69.4	71.8	24.1	87.2	84.5	40.8	69.6	66.7	57.1	55.4	76.1	95.5	67.2	70.7	70.9	86.7	85.4
$(1\alpha, 5\phi)$		69.6	71.1	24.4	88.1	83.0	42.1	72.2	66.4	57.4	57.7	75.2	95.4	67.2	70.5	70.7	86.9	85.5
$(1\alpha, 6\phi)$		69.3	70.3	23.1	87.3	83.5	38.6	74.1	65.8	56.5	57.2	76.7	95.5	65.7	70.8	71.0	86.9	85.7
$(2\alpha, 1\phi)$		67.2	70.0	19.7	84.3	86.3	39.6	65.7	62.6	52.1	50.7	73.4	95.2	64.4	69.2	71.4	86.6	84.6
$(2\alpha, 2\phi)$		67.7	70.7	25.9	84.7	84.7	37.4	65.3	63.5	52.6	53.6	71.9	95.3	65.8	69.8	71.6	86.6	84.7
$(2\alpha, 3\phi)$		68.5	70.3	19.8	86.2	86.2	38.1	70.9	64.0	55.7	55.7	74.7	95.3	65.9	69.8	72.0	87.0	84.7
$(2\alpha, 4\phi)$		69.6	72.3	24.2	86.3	85.0	41.8	72.1	66.2	56.6	56.5	76.4	95.4	66.7	70.6	71.4	86.9	85.5
$(2\alpha, 5\phi)$		69.3	72.4	21.7	86.3	84.8	40.5	68.7	66.9	56.6	58.0	76.8	95.3	67.0	70.3	71.5	86.9	85.5
$(2\alpha, 6\phi)$		69.1	71.9	20.5	87.7	84.2	41.6	69.3	66.5	56.9	55.0	76.5	95.4	66.4	70.7	71.1	86.9	85.5
$(3\alpha, 1\phi)$		67.3	70.1	20.7	82.8	86.3	34.4	66.5	62.5	53.6	55.2	74.5	95.1	64.4	69.1	71.4	86.6	84.4
$(3\alpha, 2\phi)$		68.3	71.9	16.6	85.9	83.0	39.5	66.3	66.0	57.0	56.6	76.3	95.4	64.3	70.5	71.7	86.7	84.6
$(3\alpha, 3\phi)$		68.6	70.9	20.2	86.7	86.4	39.1	68.0	66.2	56.7	53.3	74.5	95.3	66.2	70.0	71.8	87.1	85.0
$(3\alpha, 4\phi)$		68.5	70.6	19.9	86.7	86.1	39.3	67.6	66.2	56.8	54.1	74.2	95.3	65.6	70.1	71.9	87.1	84.9
$(3\alpha, 5\phi)$		69.8	72.2	24.3	87.3	84.8	41.2	73.6	67.0	57.1	55.9	76.9	95.4	67.1	70.4	71.2	86.9	85.6
$(3\alpha, 6\phi)$		69.1	71.9	20.5	87.7	84.2	41.6	69.3	66.5	56.9	55.0	76.5	95.4	66.4	70.7	71.1	86.9	85.5
$(4\alpha, 1\phi)$		66.7	70.5	15.4	85.1	86.5	35.2	67.5	62.5	51.3	51.0	72.9	95.1	63.9	68.5	71.6	86.2	84.5
$(4\alpha, 2\phi)$		68.4	70.9	18.6	86.0	85.3	39.5	69.9	65.6	56.4	54.2	73.6	95.4	65.5	70.0	71.7	87.0	84.8
$(4\alpha, 3\phi)$		68.7	70.3	22.1	86.5	86.6	39.6	67.8	66.0	57.1	53.2	75.4	95.3	66.0	69.9	71.9	87.2	85.0
$(4\alpha, 4\phi)$		68.9	71.5	23.8	86.9	83.1	38.6	74.5	65.8	56.5	50.8	75.1	95.6	65.8	70.8	70.4	87.1	85.6
$(4\alpha, 5\phi)$		69.0	71.0	23.3	87.7	83.5	40.3	73.7	66.1	56.9	51.6	75.1	95.6	65.3	70.7	70.4	87.1	85.6
$(4\alpha, 6\phi)$		69.4	70.9	25.2	87.9	83.5	40.8	73.0	66.5	57.2	54.0	76.4	95.6	65.1	70.9	70.6	87.1	85.8

Table 12: Class-wise IoU scores for granularity studies on the *voxel* representation (under 10% split on the *val* set of nuScenes [15]). All scores are given in percentage. The best score for each semantic class is highlighted in **bold**.

References

- [1] Ricardo Roriz, Jorge Cabral, and Tiago Gomes. Automotive lidar technology: A survey. *IEEE Transactions on Intelligent Transportation Systems*, 2021. 1
- [2] Andrea Censi, Konstantin Slutsky, Tichakorn Wongpiromsarn, Dmitry Yershov, Scott Pendleton, James Fu, and Emilio Frazzoli. Liability, ethics, and culture-aware behavior specification using rulebooks. In *IEEE International Conference on Robotics and Automation (ICRA)*, pages 8536–8542, 2019. 1
- [3] Scott Drew Pendleton, Hans Andersen, Xinxin Du, Xiaotong Shen, Malika Meghjani, You Hong Eng, Daniela Rus, and Marcelo H Ang. Perception, planning, control, and coordination for autonomous vehicles. *Machines*, 5, 2017. 1
- [4] Ozan Unal, Dengxin Dai, and Luc Van Gool. Scribble-supervised lidar semantic segmentation. In *IEEE/CVF Conference on Computer Vision and Pattern Recognition (CVPR)*, 2022. 1, 2, 6, 7, 9, 11, 13, 14, 18
- [5] Qingyong Hu, Bo Yang, Guangchi Fang, Yulan Guo, Ales Leonardis, Niki Trigoni, and Andrew Markham. Sqn: Weakly-supervised semantic segmentation of large-scale 3d point clouds with 1000x fewer labels. *arXiv preprint arXiv:2104.04891*, 2021. 1, 9
- [6] Biao Gao, Yancheng Pan, Chengkun Li, Sibo Geng, and Huijing Zhao. Are we hungry for 3d lidar data for semantic segmentation? a survey of datasets and methods. *IEEE Transactions on Intelligent Transportation Systems*, 2021. 1, 9
- [7] Larissa T Triess, Mariella Dreissig, Christoph B Rist, and J Marius Zöllner. A survey on deep domain adaptation for lidar perception. In *IEEE Intelligent Vehicles Symposium Workshops (IVW)*, pages 350–357, 2021. 1
- [8] David Berthelot, Nicholas Carlini, Ian Goodfellow, Nicolas Papernot, Avital Oliver, and Colin A Raffel. Mixmatch: A holistic approach to semi-supervised learning. In *Advances in Neural Information Processing Systems (NeurIPS)*, volume 32, 2019. 1, 9
- [9] Kihyuk Sohn, David Berthelot, Nicholas Carlini, Zizhao Zhang, Han Zhang, Colin A Raffel, Ekin D Cubuk, Alexey Kurakin, and Chun-Liang Li. Fixmatch: Simplifying semi-supervised learning with consistency and confidence. In *Advances in Neural Information Processing Systems (NeurIPS)*, volume 33, 2020. 1, 9
- [10] David Berthelot, Nicholas Carlini, Ekin D Cubuk, Alex Kurakin, Kihyuk Sohn, Han Zhang, and Colin Raffel. Remixmatch: Semi-supervised learning with distribution alignment and augmentation anchoring. *arXiv preprint arXiv:1911.09785*, 2019. 1, 9
- [11] Yassine Ouali, Céline Hudelot, and Myriam Tami. Semi-supervised semantic segmentation with cross-consistency training. In *IEEE/CVF Conference on Computer Vision and Pattern Recognition (CVPR)*, pages 12674–12684, 2020. 1, 14
- [12] Zhanghan Ke, Di Qiu, Kaican Li, Qiong Yan, and Rynson WH Lau. Guided collaborative training for pixel-wise semi-supervised learning. In *European Conference on Computer Vision (ECCV)*, pages 429–445, 2020. 1, 9, 14
- [13] Xiaokang Chen, Yuhui Yuan, Gang Zeng, and Jingdong Wang. Semi-supervised semantic segmentation with cross pseudo supervision. In *IEEE/CVF Conference on Computer Vision and Pattern Recognition (CVPR)*, pages 2613–2622, 2021. 1, 6, 7, 9, 14, 15, 16, 17, 18
- [14] Li Jiang, Shaoshuai Shi, Zhuotao Tian, Xin Lai, Shu Liu, Chi-Wing Fu, and Jiaya Jia. Guided point contrastive learning for semi-supervised point cloud semantic segmentation. In *IEEE/CVF International Conference on Computer Vision (ICCV)*, pages 6423–6432, 2021. 1, 6, 7, 9
- [15] Holger Caesar, Varun Bankiti, Alex H Lang, Sourabh Vora, Venice Erin Liang, Qiang Xu, Anush Krishnan, Yu Pan, Giancarlo Baldan, and Oscar Beijbom. nuscenes: A multimodal dataset for autonomous driving. In *IEEE/CVF Conference on Computer Vision and Pattern Recognition (CVPR)*, pages 11621–11631, 2020. 2, 6, 7, 9, 11, 12, 13, 14, 16, 19, 20
- [16] Jens Behley, Martin Garbade, Andres Milioto, Jan Quenzel, Sven Behnke, Cyrill Stachniss, and Juergen Gall. Semantickitti: A dataset for semantic scene understanding of lidar sequences. In *IEEE/CVF International Conference on Computer Vision (ICCV)*, pages 9297–9307, 2019. 2, 6, 7, 9, 11, 12, 13, 14, 17, 18
- [17] Andres Milioto, Ignacio Vizzo, Jens Behley, and Cyrill Stachniss. Rangenet++: Fast and accurate lidar semantic segmentation. In *IEEE/RSJ International Conference on Intelligent Robots and Systems (IROS)*, pages 4213–4220, 2019. 2, 4, 7, 9, 10
- [18] Xinge Zhu, Hui Zhou, Tai Wang, Fangzhou Hong, Yuexin Ma, Wei Li, Hongsheng Li, and Dahu Lin. Cylindrical and asymmetrical 3d convolution networks for lidar segmentation. In *IEEE/CVF Conference on Computer Vision and Pattern Recognition (CVPR)*, pages 9939–9948, 2021. 2, 4, 6, 9, 10, 11, 14

- [19] Yang Zhang, Zixiang Zhou, Philip David, Xiangyu Yue, Zerong Xi, Boqing Gong, and Hassan Foroosh. Polarnet: An improved grid representation for online lidar point clouds semantic segmentation. In *IEEE/CVF Conference on Computer Vision and Pattern Recognition (CVPR)*, pages 9601–9610, 2020. [2](#), [4](#), [7](#), [9](#), [10](#)
- [20] Hugues Thomas, Charles R Qi, Jean-Emmanuel Deschaud, Beatriz Marcotegui, Fran ois Goulette, and Leonidas J Guibas. Kpconv: Flexible and deformable convolution for point clouds. In *IEEE/CVF International Conference on Computer Vision (ICCV)*, pages 6411–6420, 2019. [2](#), [10](#)
- [21] Yiming Zhao, Lin Bai, and Xinming Huang. Fidnet: Lidar point cloud semantic segmentation with fully interpolation decoding. In *IEEE/RSJ International Conference on Intelligent Robots and Systems (IROS)*, pages 4453–4458, 2021. [2](#), [6](#), [9](#), [10](#), [13](#), [14](#)
- [22] Qingyong Hu, Bo Yang, Linhai Xie, Stefano Rosa, Yulan Guo, Niki Trigoni, Zhihua Wang, and Andrew Markham. Randla-net: Efficient semantic segmentation of large-scale point clouds. In *IEEE/CVF Conference on Computer Vision and Pattern Recognition (CVPR)*, pages 11108–11117, 2020. [2](#), [4](#), [10](#)
- [23] Yves Grandvalet and Yoshua Bengio. Semi-supervised learning by entropy minimization. In *Advances in Neural Information Processing Systems (NeurIPS)*, volume 17, 2004. [3](#)
- [24] Hongyi Zhang, Moustapha Cisse, Yann N. Dauphin, and David Lopez-Paz. mixup: Beyond empirical risk minimization. In *International Conference on Learning Representations (ICLR)*, 2018. [4](#), [7](#)
- [25] Sangdoo Yun, Dongyoon Han, Seong Joon Oh, Sanghyuk Chun, Junsuk Choe, and Youngjoon Yoo. Cutmix: Regularization strategy to train strong classifiers with localizable features. In *IEEE/CVF International Conference on Computer Vision (ICCV)*, pages 6023–6032, 2019. [4](#), [7](#)
- [26] Antti Tarvainen and Harri Valpola. Mean teachers are better role models: Weight-averaged consistency targets improve semi-supervised deep learning results. In *Advances in Neural Information Processing Systems (NeurIPS)*, volume 30, 2017. [5](#), [6](#), [7](#), [8](#), [9](#), [14](#), [15](#), [16](#), [17](#), [18](#)
- [27] Dong-Hyun Lee. Pseudo-label: The simple and efficient semi-supervised learning method for deep neural networks. In *International Conference on Machine Learning Workshops (ICMLW)*, volume 3, 2013. [5](#), [9](#)
- [28] Avital Oliver, Augustus Odena, Colin A Raffel, Ekin D Cubuk, and Ian Goodfellow. Realistic evaluation of deep semi-supervised learning algorithms. In *Advances in Neural Information Processing Systems (NeurIPS)*, volume 31, 2018. [6](#)
- [29] Geoff French, Timo Aila, Samuli Laine, Michal Mackiewicz, and Graham Finlayson. Semi-supervised semantic segmentation needs strong, high-dimensional perturbations. In *British Machine Vision Conference (BMVC)*, 2020. [6](#), [7](#), [9](#), [14](#), [16](#), [17](#), [18](#)
- [30] Yang Zou, Zhiding Yu, B V K Vijaya Kumar, and Jinsong Wang. Unsupervised domain adaptation for semantic segmentation via class-balanced self-training. In *European Conference on Computer Vision (ECCV)*, pages 289–305, 2018. [6](#), [7](#), [9](#), [14](#), [16](#), [17](#), [18](#)
- [31] Tiago Cortinhal, George Tzelepis, and Eren Erdal Aksoy. Salsanext: Fast, uncertainty-aware semantic segmentation of lidar point clouds for autonomous driving. *arXiv preprint arXiv:2003.03653*, 2020. [7](#), [9](#), [10](#)
- [32] Qi Chen, Sourabh Vora, and Oscar Beijbom. Polarstream: Streaming lidar object detection and segmentation with polar pillars. In *Advances in Neural Information Processing Systems (NeurIPS)*, 2021. [7](#), [10](#)
- [33] Terrance DeVries and Graham W. Taylor. Improved regularization of convolutional neural networks with cutout. *arXiv preprint arXiv:1708.04552*, 2017. [7](#)
- [34] Chenfeng Xu, Bichen Wu, Zining Wang, Wei Zhan, Peter Vajda, Kurt Keutzer, and Masayoshi Tomizuka. Squeezesegv3: Spatially-adaptive convolution for efficient point-cloud segmentation. In *European Conference on Computer Vision (ECCV)*, pages 1–19, 2020. [9](#), [10](#)
- [35] Haotian Tang, Zhijian Liu, Shengyu Zhao, Yujun Lin, Ji Lin, Hanrui Wang, and Song Han. Searching efficient 3d architectures with sparse point-voxel convolution. In *European Conference on Computer Vision (ECCV)*, pages 685–702, 2020. [9](#), [10](#)
- [36] Yuenan Hou, Xinge Zhu, Yuexin Ma, Chen Change Loy, and Yikang Li. Point-to-voxel knowledge distillation for lidar semantic segmentation. In *IEEE/CVF Conference on Computer Vision and Pattern Recognition (CVPR)*, pages 8479–8488, 2022. [9](#)
- [37] Venice Erin Lioung, Thi Ngoc Tho Nguyen, Sergi Widjaja, Dhananjai Sharma, and Zhuang Jie Chong. Amvnet: Assertion-based multi-view fusion network for lidar semantic segmentation. *arXiv preprint arXiv:2012.04934*, 2020. [9](#)
- [38] Jianyun Xu, Ruixiang Zhang, Jian Dou, Yushi Zhu, Jie Sun, and Shiliang Pu. Rpvnet: A deep and efficient range-point-voxel fusion network for lidar point cloud segmentation. In *IEEE/CVF International Conference on Computer Vision (ICCV)*, pages 16024–16033, 2021. [9](#)

- [39] Yachao Zhang, Yanyun Qu, Yuan Xie, Zonghao Li, Shanshan Zheng, and Cuihua Li. Perturbed self-distillation: Weakly supervised large-scale point cloud semantic segmentation. In *IEEE/CVF International Conference on Computer Vision (ICCV)*, pages 15520–15528, 2021. [9](#)
- [40] Yan Liu, Qingyong Hu, Yinjie Lei, Kai Xu, Jonathan Li, and Yulan Guo. Box2seg: Learning semantics of 3d point clouds with box-level supervision. *arXiv preprint arXiv:2201.02963*, 2022. [9](#)
- [41] Jilin Mei, Biao Gao, Donghao Xu, Wen Yao, Xijun Zhao, and Huijing Zhao. Semantic segmentation of 3d lidar data in dynamic scene using semi-supervised learning. *IEEE Transactions on Intelligent Transportation Systems*, 21(6):2496–2509, 2019. [9](#)
- [42] Minghua Liu, Yin Zhou, Charles R Qi, Boqing Gong, Hao Su, and Dragomir Anguelov. Less: Label-efficient semantic segmentation for lidar point clouds. In *IEEE/CVF Conference on Computer Vision and Pattern Recognition (CVPR)*, 2022. [9](#)
- [43] Samuli Laine and Timo Aila. Temporal ensembling for semi-supervised learning. In *International Conference on Learning Representations (ICLR)*, 2017. [9](#)
- [44] Yuliang Zou, Zizhao Zhang, Han Zhang, Chun-Liang Li, Xiao Bian, Jia-Bin Huang, and Tomas Pfister. Pseudoseg: Designing pseudo labels for semantic segmentation. In *International Conference on Learning Representations (ICLR)*, 2020. [9](#)
- [45] Yuyuan Liu, Yu Tian, Yuanhong Chen, Fengbei Liu, Vasileios Belagiannis, and Gustavo Carneiro. Perturbed and strict mean teachers for semi-supervised semantic segmentation. *arXiv preprint arXiv:2111.12903*, 2021. [9](#)
- [46] Jianlong Yuan, Yifan Liu, Chunhua Shen, Zhibin Wang, and Hao Li. A simple baseline for semi-supervised semantic segmentation with strong data augmentation. In *IEEE/CVF International Conference on Computer Vision (ICCV)*, pages 8229–8238, 2021. [9](#)
- [47] Viktor Olsson, Wilhelm Tranheden, Juliano Pinto, and Lennart Svensson. Classmix: Segmentation-based data augmentation for semi-supervised learning. In *IEEE/CVF Winter Conference on Applications of Computer Vision (WACV)*, pages 1369–1378, 2021. [9](#)
- [48] Wenfeng Luo and Meng Yang. Semi-supervised semantic segmentation via strong-weak dual-branch network. In *European Conference on Computer Vision (ECCV)*, pages 784–800, 2020. [9](#)
- [49] Lihe Yang, Wei Zhuo, Lei Qi, Yinghuan Shi, and Yang Gao. St++: Make self-training work better for semi-supervised semantic segmentation. In *IEEE/CVF Conference on Computer Vision and Pattern Recognition (CVPR)*, 2022. [9](#)
- [50] Whye Kit Fong, Rohit Mohan, Juana Valeria Hurtado, Lubing Zhou, Holger Caesar, Oscar Beijbom, and Abhinav Valada. Panoptic nuscenes: A large-scale benchmark for lidar panoptic segmentation and tracking. *IEEE Robotics and Automation Letters*, pages 3795–3802, 2022. [9](#), [13](#)
- [51] Amit Pal Singh Kohli, Vincent Sitzmann, and Gordon Wetzstein. Semantic implicit neural scene representations with semi-supervised training. In *IEEE International Conference on 3D Vision (3DV)*, pages 423–433, 2020. [9](#)
- [52] Chun-Yu Sun, Yu-Qi Yang, Hao-Xiang Guo, Peng-Shuai Wang, Xin Tong, Yang Liu, and Heung-Yeung Shum. Semi-supervised 3d shape segmentation with multilevel consistency and part substitution. *arXiv preprint arXiv:2204.08824*, 2022. [9](#)
- [53] Shuang Deng, Qilei Dong, Bo Liu, and Zhanyi Hu. Superpoint-guided semi-supervised semantic segmentation of 3d point clouds. *arXiv preprint arXiv:2107.03601*, 2021. [9](#)
- [54] Mingmei Cheng, Le Hui, Jin Xie, and Jian Yang. Sspc-net: Semi-supervised semantic 3d point cloud segmentation network. In *AAAI Conference on Artificial Intelligence (AAAI)*, pages 1140–1147, 2021. [9](#)
- [55] Alexey Nekrasov, Jonas Schult, Or Litany, Bastian Leibe, and Francis Engelmann. Mix3D: Out-of-Context Data Augmentation for 3D Scenes. In *International Conference on 3D Vision (3DV)*, pages 116–125, 2021. [9](#)
- [56] Jianren Wang, Haiming Gang, Siddarth Ancha, Yi-Ting Chen, and David Held. Semi-supervised 3d object detection via temporal graph neural networks. In *IEEE International Conference on 3D Vision (3DV)*, pages 413–422, 2021. [9](#)
- [57] Jinhyung Park, Chenfeng Xu, Yiyang Zhou, Masayoshi Tomizuka, and Wei Zhan. Detmatch: Two teachers are better than one for joint 2d and 3d semi-supervised object detection. *arXiv preprint arXiv:2203.09510*, 2022. [9](#)
- [58] Charles R Qi, Yin Zhou, Mahyar Najibi, Pei Sun, Khoa Vo, Boyang Deng, and Dragomir Anguelov. Offboard 3d object detection from point cloud sequences. In *IEEE/CVF Conference on Computer Vision and Pattern Recognition (CVPR)*, pages 6134–6144, 2021. [9](#)
- [59] Charles R Qi, Hao Su, Kaichun Mo, and Leonidas J Guibas. Pointnet: Deep learning on point sets for 3d classification and segmentation. In *IEEE/CVF Conference on Computer Vision and Pattern Recognition (CVPR)*, pages 652–660, 2017. [10](#)

- [60] Ilya Loshchilov and Frank Hutter. Decoupled weight decay regularization. In *International Conference on Learning Representations (ICLR)*, 2018. [14](#)
- [61] Leslie N. Smith and Nicholay Topin. Super-convergence: Very fast training of neural networks using large learning rates. *arXiv preprint arXiv:1708.07120*, 2017. [14](#)
- [62] Marius Cordts, Mohamed Omran, Sebastian Ramos, Timo Rehfeld, Markus Enzweiler, Rodrigo Benenson, Uwe Franke, Stefan Roth, and Bernt Schiele. The cityscapes dataset for semantic urban scene understanding. In *IEEE/CVF Conference on Computer Vision and Pattern Recognition (CVPR)*, pages 3213–3223, 2016. [14](#)